PLASMA DYNAMICS

X. PLASMA PHYSICS*

Prof. S. C. Brown
Prof. W. P. Allis
Prof. G. Bekefi
Prof. K. U. Ingard
Prof. D. R. Whitehouse
Dr. J. C. Ingraham
Dr. G. Lampis
M. L. Andrews
F. X. Crist
J. K. Domen
E. W. Fitzgerald, Jr.
G. A. Garosi
K. W. Gentle
E. V. George
W. H. Glenn, Jr.
E. B. Hooper, Jr.
P. W. Jameson
R. L. Kronquist
D. T. Llewellyn-Jones
E. M. Mattison
J. J. McCarthy
W. J. Mulligan
J. J. Nolan, Jr.
L. D. Pleasance
G. L. Rogoff
D. W. Swain
F. Y-F. Tse
B. L. Wright

A. ON THE AMBIPOLAR TRANSITION

A report[1] by Cohen and Kruskal (referred to here as C+K) considers the ambipolar transition by dividing the problem into a number of "regions" in which the equations may be simplified, and this is very helpful in understanding the problem. The report is, however, difficult to follow for a number of reasons, and it therefore appears useful to write the present report, containing little that is factually different from theirs, but in which some more complete equations are presented and the structure of the problem is more carefully exhibited. The method of C+K makes mathematical rigor possible, which is excellent, but the report is not convincing that the rigor is always there. Hidden errors may lurk where the interrelations of equations are not clearly shown. C+K consider various limiting forms assumed by the complete ambipolar diffusion equations when certain parameters go to zero or infinity. In each case the limiting process results in dropping one term in each of several three-term equations. In any physical problem where parameters and variables may have values ranging over orders of magnitude it is generally true that, to some approximation, the smallest term out of three may be neglected. In this problem the three terms A, B, C, will be of the same sign, so that the full equation can be written

$$A + B = C \tag{AB}$$

with two simplified forms

$$A = C \tag{A}$$

or

$$B = C \tag{B}$$

These simplified forms will be called "limits" in the sense that some physical process has become inoperative when a term can be dropped. This is different from the mathematical meaning of "limit" used by C+K, although the result is generally the same. The

*This work was supported by the United States Atomic Energy Commission (Contract AT(30-1)-1842).

full equation (AB) will be called a "transition" and must be used in the neighborhood of A = B. In a "transition" two physical processes are competing.

As there will be 3 three-term equations, there are 8 possible limits, but as we shall assume that the positive ions are both heavier and colder than the electrons, only 4 of the limits actually occur. They will be named, somewhat arbitrarily, the Ambipolar (a), Boltzmann (b), Cosine (c), and Diffusion (d) limits. These will be discussed in reverse order. They are separated by the Space-Charge (ab), Electron-Flow (bc), and Ion-Flow (cd) transitions. We also consider the sheath limit (s) in which ionization is neglected.

It must not be assumed that the same limit holds throughout a given plasma. In general, the transition condition A = B will cut across the diffusing, and therefore nonuniform, plasma so that several limiting and transition forms must be used. It is our purpose to sketch the way in which these limiting and transition forms fit together in a given plasma. This leads to our final diagram (Fig. X-3) which summarizes as much information as can be collected in a single figure.

In order to facilitate comparison with the work of C+K their equation number (D._._) or the page reference (Eq._p._) will be given next to ours whenever we have found the appropriate reference.

(e) Basic Equations

The physical parameters of this problem are the ion and electron temperatures $T_\pm$ and transport coefficients $\mu_\pm$, $D_\pm = \mu_\pm T_\pm$, the ionization frequency ν_i, and the diffusion length $\Lambda = L/\pi$. Parallel plane geometry will be considered. These physical parameters are combined in the following dimensionless parameters:

$$\tau = T_+/T_- \leqslant 1$$

$$\mu = \mu_+/\mu_- < 1$$

$$\delta = D_+/D_- = \tau\mu \ll 1 \qquad \text{(e 1) (p. 15)}$$

$$\nu = \nu_i\Lambda^2/T_-\mu_+$$

and use will also be made of the electric field $\mathscr{E}_i$ defined as

$$\mathscr{E}_i^2 = \nu_i T_-/\mu_+. \qquad \text{(e 2)}$$

(Note that our τ is $1/\tau$ in C+K.) The first three parameters are less than 1, the fourth is a characteristic value obtained from the solution of the equations. Its free and ambipolar limits are $1/\mu$ and $(1+\tau)/(1+\mu)$; C+K claim that this last limit is approached <u>from below</u>. We claim this has not been proved.

We then introduce the dimensionless variables

$$
\begin{aligned}
n_{\pm} &= N_{\pm} e\mu_{+}/\epsilon_{o}\nu_{i} \\
s &= n_{+} - n_{-} \\
E &= \mathscr{E}/\mathscr{E}_{i} \\
J &= \Gamma_{e}/\epsilon_{o}\mathscr{E}_{i}\nu_{i} \\
x &= X\mathscr{E}_{i}/T_{-}
\end{aligned}
\qquad \text{(e 3) (p. 15)}
$$

and use the same variables throughout. They differ slightly from the variables used by Allis and Rose[2] (referred to here as A+R). C+K rescale variables on pp. 33, 37, 38, 45, 59, 60, 71 and this makes their equations difficult to compare. Our single set of variables resembles their barred variables but differs from them by factors of $\pi/2$ because of the use of the diffusion length Λ in the dimensionless parameters (e 1). Ours are chosen so that τ and μ tag those terms in the equations which are going to be neglected and that ν not appear explicitly in the equations. They are all of order 1 at the space-charge transition.

In terms of these variables, the ion flow, electron flow, Poisson and ion generation equations are

$$
\begin{aligned}
J &= -\tau\nabla n_{+} + En_{+} \\
\mu J &= -\nabla n_{-} - En_{-} \\
\nabla \cdot E &= n_{+} - n_{-} = s \\
\nabla \cdot J &= n_{-}
\end{aligned}
\qquad \text{(e 4) (B. 1)}
$$

with the boundary conditions

$$
\begin{aligned}
&n_{-} = n_{o} \qquad n_{+} = n_{+o} \qquad \text{at } J = E = x = 0 \\
&J = J_{d},\ E = E_{d},\ x = x_{d} \qquad \text{at } n_{-} = n_{+} = 0.
\end{aligned}
\qquad \text{(e 5)}
$$

The reason for the subscript d at the wall will appear later. Here, n_o is quite arbitrary but n_{+o}/n_o is determined a posteriori by requiring that n_+ and n_- go to zero at the same place. J_d, E_d, and x_d have whatever values result from the solution. By requiring that x_d correspond to $X = L/2$ at the wall, it follows from (e 1) and (e 3) that in these variables

$$\sqrt{\nu} = 2x_{d}/\pi. \qquad \text{(e 6)}$$

Thus the characteristic value is computed directly without the need of any fitting.

The set of equations (e 4) is assumed to be valid all the way to the wall, which implies that the collision mean-free path is much smaller than the thickness of any boundary

layer. This is rarely true, but the assumption provides definiteness to the mathematical problem.

Because the equations are invariant to translations in x, it is convenient to eliminate it as independent variable in favor of the current, J (p. 38). This is done by use of the ion-generation equation and leads to the set of 3 three-term equations mentioned above. Primes are used for derivatives with respect to J.

$$\begin{aligned} -\tau n_- n_+' &= J - E n_+ \\ -n_- n_-' &= \mu J + E n_- \\ n_- E' &= n_+ - n_- \end{aligned} \qquad \text{(e 7)}$$

The space coordinate is then obtained by quadrature

$$x = \int_o \frac{dJ}{n_-} = \int^{n_o} \frac{dn_-}{\mu J + E n_-}. \qquad \text{(e 8)}$$

Certain exact relations can be derived from the set of equations (e 7), and in order to be perfectly clear as to which equations are exact, they are all summarized here. Limit solutions can then be compared with them to see explicitly what has been neglected. Taking the derivative of the ion flow equation and combining with Poisson's equation gives

$$\left(\frac{n_+}{n_-} - 1\right) n_+ = 1 - E n_+' + \tau(n_- n_+'). \qquad \text{(e 9)}$$

Combining the equations in different ways yields the two relations that are useful near the ambipolar limit

$$(1-\delta)J - (1+\tau)E n_- = Es - \tau n_- s' \qquad \text{(e 10) (D. 3. 5)}$$

$$(1+\mu)J + (1+\tau)n_- n_-' = Es - \tau n_- s' = \sigma. \qquad \text{(e 11) (D. 3. 8)}$$

Eliminating J from the flow equations, combining with Poisson's equation, and integrating gives

$$\frac{1}{2}\mu E^2 + (1+\mu)\int_o E\, dJ = n_o - n_- - \delta(n_{+o} - n_+). \qquad \text{(e 12)}$$

A somewhat different combination of the equations yields, upon integrating,

$$\left(J + \frac{\mu E}{1+\mu}\right)^2 = \frac{1+\tau}{1+\mu}(n_o n_{+o} - n_- n_+) + \frac{2\mu}{1+\mu}[n_o - n_- - (n_{+o} - n_+)] + \frac{1-\tau}{1+\mu}\int^{n_o} (n_+\, dn_- - n_-\, dn_+). \qquad \text{(e 13)}$$

For an isothermal plasma $\tau = 1$, so that the integral in (e 13) drops out and the remaining terms are a first integral of the equations.

Finally, n_- can be divided out of (e 11) so that it integrates with respect to $dJ = n_- dx$.

$$(1+\mu) \int_o J\, dx = E^2/2 + n_o - n_- + \tau(n_{+o} - n_+) \qquad \text{(e 14)}$$

$$(1+\mu) \int_o^{Xd} J\, dx = E_d^2/2 + n_o + \tau n_{+o}. \qquad \text{(e 15)}$$

(d) Diffusion Limit $\quad \mu_- \to \mu_+ \to 0 \quad n_+ \ll \delta$

In the limit of very low densities the quadratic terms En_+ and En_- can be neglected so that the limiting equations are

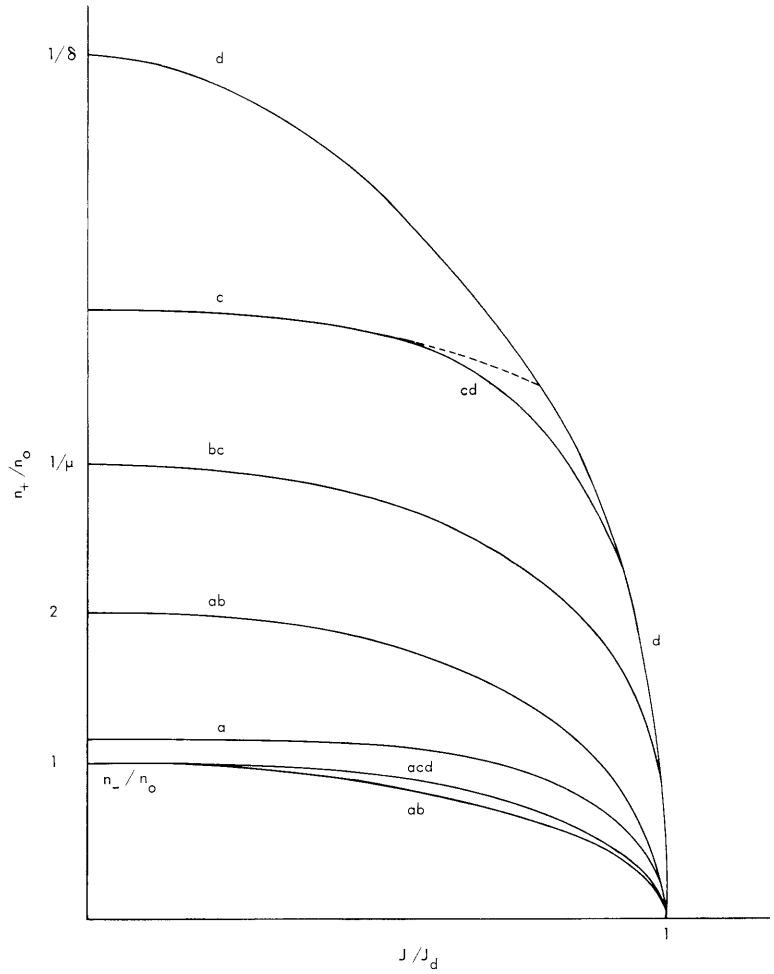

Fig. X-1. Plasma profiles.

$$-\tau n_- n_+' = J$$

$$-n_- n_-' = \mu J \qquad \text{(d 1)}$$

$$n_- E' = n_+ - n_-,$$

and the solution is

$$\delta n_+ = n_-$$

$$\delta E = (1-\delta)J \qquad \text{(d 2) (D. 4. 3)}$$

$$\mu J^2 = n_o^2 - n_-^2$$

$$n_- = n_o \cos \sqrt{\mu}\, x \qquad \text{(d 3)}$$

$$\nu = \nu_d = 1/\mu.$$

It will be convenient to plot n_-/n_o and n_+/n_o against J/J_d (see Fig. X-1). Both plots are ellipses in this limit and remain identical for all sufficiently small values of n_o. As C+K show quite generally that

$$\delta n_+ \leq n_- \leq n_+, \qquad \text{(d 4) (B. 6)}$$

all future curves of n_+/n_o will fall between these two limit curves.

Putting the value of E from (d 2) into the electron flow equation (e 7) yields the first-order departure

$$\sqrt{\mu\nu} = 1 - \frac{2}{3\pi} \frac{1-\delta}{\delta} \frac{n_o}{\mu}. \qquad \text{(d 5) (p. 75)}$$

(cd) Ion Flow Transition $\qquad \mu_- \to n_-/n_+ \to 0 \qquad n_{+o} \approx \delta$

As $En_-/\mu En_+ \approx \tau$, and we assume $\tau < 1$, the ion mobility term will, with increasing density, become equal to and cross the ion diffusion term before the electron mobility term need be considered. In an active plasma the electric field assists the ions to flow out before it effectively retains the electrons. This is the Ion Flow Transition. It occurs before the Electron Flow Transition in an active plasma, although they occur together in an isothermal plasma. We shall consider them separately. The appropriate equations for the Ion Flow Transition are

$$-\tau n_- n_+' = J - En_+$$

$$-n_- n_-' = \mu J \qquad \text{(cd 1)}$$

$$n_- E' = n_+.$$

From (e 12) we see that

$$\frac{1+\tau}{2}\mu E^2 = n_o - n_- - \delta(n_{+o}-n_+), \qquad \text{(cd 2) (D. 2. 4)}$$

and from the electron flow equation, as before,

$$\begin{aligned} \mu J^2 &= n_o^2 - n_-^2 \\ \mu\nu &= 1. \end{aligned} \qquad \text{(cd 3)}$$

(c) Cosine Limit $\qquad D_+ \to n_-/n_+ \to 0 \qquad \delta < n_{+o} < \mu$

After the ion flow transition, the appropriate equations are

$$\begin{aligned} J &= En_+ \\ -n_-n_-' &= \mu J \\ n_-E' &= n_+. \end{aligned} \qquad \text{(c 1)}$$

The electron profile is the same as before

$$\begin{aligned} \mu J^2 &= n_o^2 - n_-^2 \\ \mu\nu &= 1, \end{aligned} \qquad \text{(cd 3)}$$

but now we have

$$\frac{1}{2}\mu E^2 = n_o - n_- \qquad \text{(D. 2. 8)}^*$$

$$n_+^2 = (n_o+n_-)/2 \qquad \text{(c 2)}$$

$$n_+ = \sqrt{n_o}\cos\sqrt{\mu}\, x/2. \qquad \text{(D. 2. 7)}$$

[*In going from (D. 2. 4) to (D. 2. 8) C+K neglect δn_{+o} but keep δn_+. This seems inconsistent.]

This limit has been called the Cosine Limit because n_+ is a cosine function; but it is of twice the base, so that it does not vanish at the wall. Clearly this limit, as all of the regions that follow, are not valid beyond the point where their plasma profiles intersect the curve (d) of Fig. X-1. The solutions (c 2) must be broken off at a coordinate $x_c < x_d$ at which the conditions of validity of (c 1) break down and a single new boundary condition of the form

$$n_-/n_+ = c \qquad \text{(c 3)}$$

must replace (e 5).

The impossibility of satisfying the double boundary condition $n_+ = n_- = 0$ arises because in dropping the ion diffusion term the order of the equations has been reduced by one, and hence there is one less disposable constant of integration. This becomes obvious when we drop the diffusion term in (e 9). This then becomes

$$\frac{n_+}{n_-} = 1 + \frac{1 - En'_+}{n_+} \geq 1 + \frac{1}{n_+} \tag{c 4}$$

and

$$\frac{n_{+o}}{n_o} = 1 + \frac{1}{n_{+o}}. \tag{c 5}$$

Thus n_o and n_{+o} are related by (c 5) and only one of them may be chosen arbitrarily. Thus we no longer have the flexibility to require both n_+ and n_- to go to zero. In fact, neither one can go to zero before the conditions of the equation set (c 1) become invalid. (The appropriate constant in (c 3) will be discussed below in (s) Sheaths.) We also have a bound on n_+/n_- and it is now convenient to represent the solutions as plots of n_-/n_+

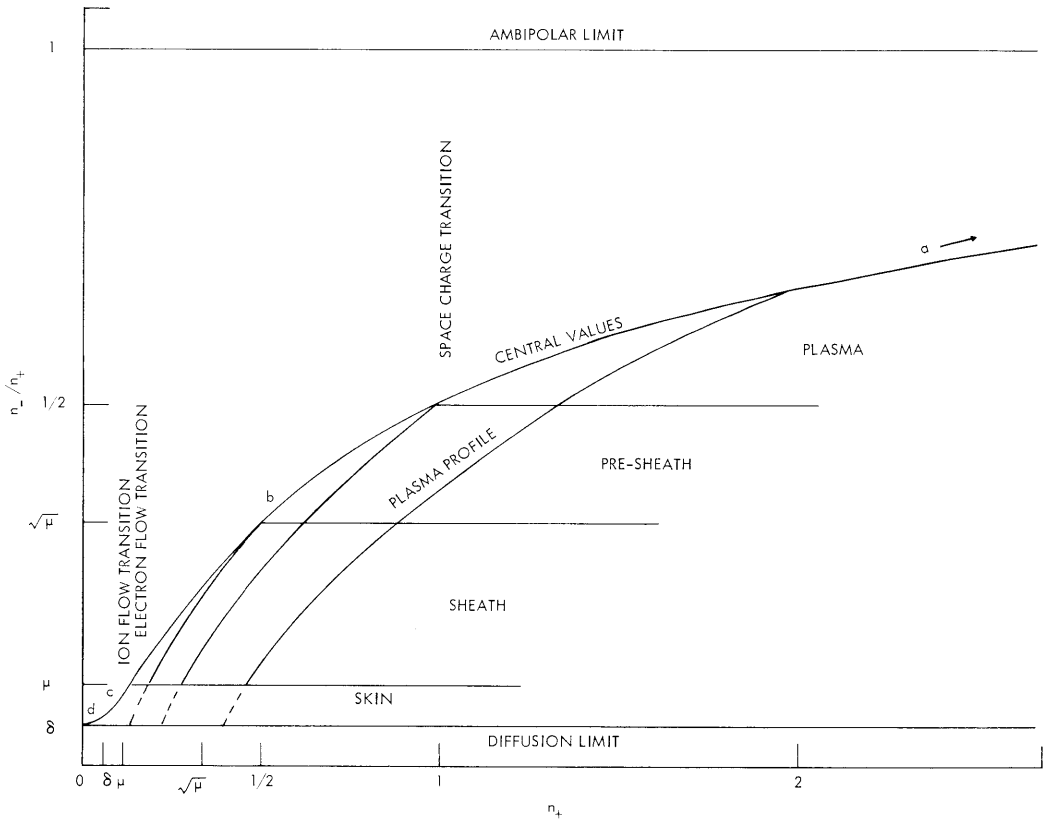

Fig. X-2. Plasma ratios.

against n_+ (Fig. X-2). For $n_+ > \delta$ all of the integral curves start on the hyperbola (c 4) at $n_+ = n_{+o}$ and remain below it. Eventually they curve sharply to the left, because of the ion diffusion term, and meet the axis of ordinates at $n_-/n_+ = \delta$. In practice, it may often be sufficient simply to cut the curves off at $n_-/n_+ = \delta$ without computing the ion diffusion part.

Note that (c 4) and (c 5) remain valid through (c), (b), and (a). Similarly, the electron profile (cd 3) remained valid through (d) and (c). The formula (d 5) produces a hardly noticeable change in ν through these regions. After (c) it is not the appropriate formula. We should now take E from (c 2) and put it into the electron-flow equation to get first-order departures for ν. This yields

$$\sqrt{\mu\nu} = 1 - \frac{2.13}{\pi}\frac{\sqrt{n_o}}{\mu}, \qquad \text{(c 6)}$$

where the decimal comes from a complicated logarithmic term. This differs markedly from the previous formula (d 5) and is valid for considerably larger values of n_o.

(bc) Electron-Flow Transition $\qquad D_+ \to n_-/n_+ \to 0 \qquad n_{+o} \approx \mu$

The next term to enter the equations is the electron mobility, which acts to oppose the electron flow. The equations then are

$$\begin{aligned} J &= En_+ \\ -n_-n_-' &= J + En_- \qquad \text{(bc 1)} \\ n_-E' &= n_+. \end{aligned}$$

A relatively simple equation can be obtained for the current squared $J^2 = F$ in terms of the field squared $E^2 = Y$. The equation is

$$2F'' + \sqrt{\frac{Y}{F}}\,F' + \mu = 0, \qquad \text{(bc 2) (D. 2. 11)}$$

where the primes are derivatives with respect to Y, with

$$\begin{aligned} n_+ &= \sqrt{F/Y} \\ n_- &= F'. \end{aligned}$$

A similar equation has been solved by C+K.

(b) Boltzmann Limit $\qquad D_+ \to n_-/n_+ \to 0 \qquad \mu \to \infty \qquad \mu < n_{+o} < 1$

In this limit the ions are cold, flow is due to the field only, and the electrons have such large mobility that they assume a Boltzmann distribution in the field

$$n_- = n_o e^{-V}. \tag{b 1}$$

The equations are

$$\begin{aligned} J &= En_+ \\ -n_-' &= E \\ n_- E' &= n_+ \end{aligned} \tag{b 2}$$

and they lead to the simple equation

$$J = nn'n''. \tag{b 3} \text{ (D. 1. 9)}$$

This limit is called the "Similarity Solution" by C+K because it has an obvious scaling law:

$$\begin{aligned} n_- &\to k^4 n_- & J &\to k^3 J \\ n_+ &\to k^2 n_+ & E &\to kE \\ x &\to s/k & \nu &\to \nu/k^2 \\ N_+ &= \text{const} & N_- \nu_i &= \text{const.} \end{aligned} \tag{b 4} \text{ (Eq. 3 p. 43)}$$

Here, the last line makes use of definitions (e 1) and (e 3). This implies that when N_o varies in the range of validity of (b), which is two decades in Fig. 5 of C+K, ν_i varies inversely with N_o, and N_+ does not change at all! Fortunately there is a fallacy in this argument. The boundary condition (c 3) does not satisfy the scaling law. Hence x_c does not scale with x, and nothing can be said about the scaling of ν. The result on p. 43 of C+K is difficult to understand.

(ab) Space Charge Transition $\quad D_+ \to 0 \quad \mu_- \to \infty \quad n_{+o} \approx 1$

In the regions considered thus far with $n_+ < 1$ it follows from (c 4) that $n_-/n_+ < 1/2$ and hence the electron space charge could, in the approximation used throughout this report, be neglected. It must now be included and the equations are

$$\begin{aligned} J &= En_+ \\ -n_-' &= E \end{aligned} \tag{ab 1}$$

$$n_+ = n_-(1+E') = n_-(1-n_-'') \tag{D. 1. 7}$$

which yield

$$J = n_- n_-'(n_-''-1). \tag{ab 2} \text{ (D. 1. 8)}$$

The electron profiles plotted against x are bell-shaped with an inflection at $E^2 = s$. As E is large near the wall, the profile against J comes in to the axis nearly vertically, so that its departure from ellipticity is unnoticeable.

Note that the equations now contain no physical parameters. They are universal, and tabulated solutions with n_o as a parameter would be very useful; it is left to the user to join these solutions to the boundary solutions appropriate to his problem.

(a) Ambipolar Limit $\quad n_+/n_- \to 1 \quad n_o > 1$

In this limit the Poisson term is neglected. As the electron current and ion diffusion terms do not create extra difficulties, it is convenient to re-introduce them. The equations, therefore, are

$$-\tau n_- n_+' = J - En_+$$

$$-n_- n_+' = \mu J + En_- \qquad \text{(a 1) (D. 3. 2)}$$

$$n_+ = n_-$$

and the solution is

$$(1-\delta)J = (1+\tau)En_-$$

$$(1-\mu)J^2 = (1+\tau)\left(n_o^2 - n_-\right) \qquad \text{(a 2) (pp. 44 + 45)}$$

$$n = n_o \cos \sqrt{\frac{1+\mu}{1+\tau}}\, x \qquad \text{(D. 3. 3)}$$

$$\nu = \nu_a = \frac{1+\tau}{1+\mu}.$$

Computing the Poisson term, one finds

$$n_- E' = \frac{1-\delta}{1+\mu}\left(\frac{n_o}{n_-}\right)^2 = s. \qquad \text{(a 3)}$$

For equations (a 1) to be valid one must have

$$s < n_- \qquad \text{(a 4)}$$

or

$$n_-^3 > n_{ab}^2 = n_o^2 \qquad \text{(Eq. 3, p. 45)}$$

and the ambipolar limit is perhaps best expressed as

$$\text{limit } n_-^3/n_o^2 \to \infty. \qquad \text{(a 5)}$$

The ambipolar transition takes place first at the center and works outward, never reaching the wall.

From (a 3) we see that there is a space charge $s_o = (1-\delta)/(1+\mu)$ at the center of the plasma and the space charge at the wall is much larger, although (a 3) is clearly excessive. It is interesting to know how large the effect of the distributed space charge is compared with that in the sheath.

Making use of (a 3) and neglecting terms in s^2/n_-^2, one finds that the right-hand side of (e 11) is

$$\sigma = -(1+\tau)\alpha s n', \tag{a 6}$$

where

$$\alpha = \frac{1 - 2\tau - 3\delta}{(1+\tau)(1+\mu)},$$

so that

$$(1+\mu)J^2 = (1+\tau)(n_o+n_-+2\alpha\bar{s})(n_o-n_-) \tag{a 7}$$

and $\bar{s}$ is a number between s_o and s.

Treating s as constant in (a 6) and integrating dJ/n_- from n_o to n_a gives

$$\frac{x}{\sqrt{\nu_a}} = \frac{\pi}{2} - \sin^{-1}\frac{n_a + \alpha\bar{s}}{n_o + \alpha\bar{s}} + \frac{\alpha s}{n_o}\ln\frac{2n_o}{n_a}$$

$$\rightarrow \frac{\pi}{2} - \frac{n_a}{n_o} + \frac{\alpha s}{n_o}\ln\frac{2n_o}{en_a}, \tag{a 8}$$

where $e = 2.718$. Hence

$$\sqrt{\frac{\nu}{\nu_a}} \approx 1 + \frac{2}{\pi n_o}\left(\alpha s \ln\frac{2n_o}{en_a} - n_a\right). \tag{a 9}$$

There is a negative effect on ν because of cutting off the integral at n_a instead of at zero and a positive effect caused by the space charge. The first will be partially or totally offset by adding the sheath thickness. The space-charge term is already dominant if $\bar{s}$ is given its value (a 3) at n_a, but not if given the value s_o. There is a larger space charge, however, in the sheaths. The effect of this sheath charge will have to be added to the effect computed here.

(s) Sheaths $\quad J = J_d$

None of the limits (c) to (a) are valid out to the boundary of the plasma. As n_o increased and successive approximations became valid in the center, the previous

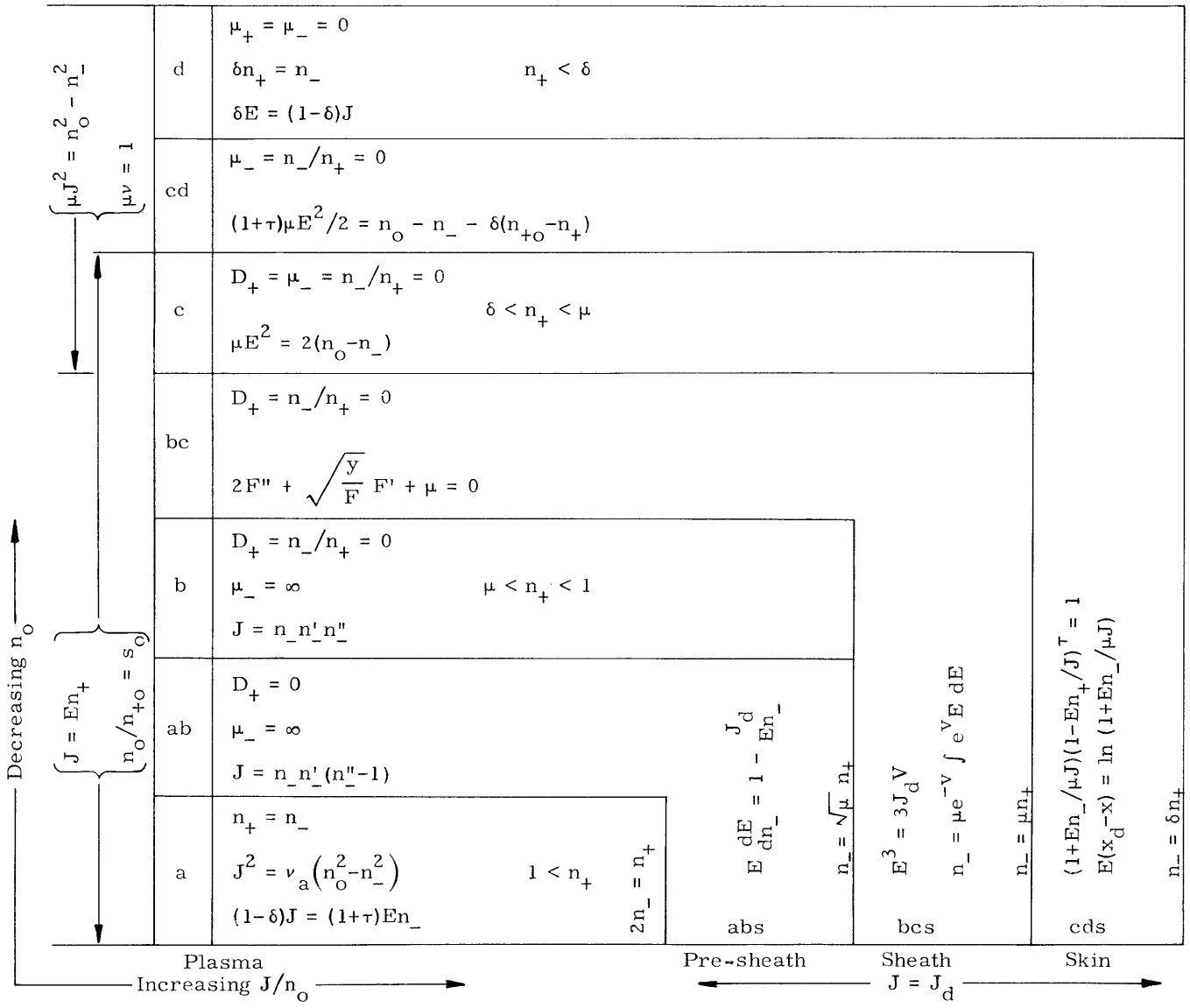

Fig. X-3. Diagrammed solutions of the ambipolar equations.

regions were merely pushed out toward the wall in successive layers. As they approach the wall, a new approximation becomes valid: the current through them becomes substantially constant. The current is therefore no longer a suitable independent variable in the equations, and we turn to the variable E by dividing each equation (e 7) by Poisson's equation:

$$\tau \frac{dn_+}{dE} = \frac{-J_d + En_+}{n_+ - n_-} \tag{s 1}$$

$$\frac{dn_-}{dE} = \frac{-\mu J_d - En_-}{n_+ - n_-} \tag{s 2}$$

$$x_s = \int \frac{dE}{n_+ - n_-}. \tag{s 3}$$

The crowding toward the wall is evident in Fig. X-1 where all the profiles crowd together at $J = J_d$. Figure X-3 is a diagram based on Fig. X-1 but distorted to show how the central regions are bounded toward the wall. Thus we see that the total sheath region may be divided into three parts: a pre-sheath, a sheath, and a skin.

(abs) Pre-Sheath $\quad D_+ \to 0 \quad \mu_- \to \infty \quad \sqrt{\mu} < n_-/n_+ < 1/2$

This is an extension of the space-charge transition region. It is the region that is well known to prove theorists in which electron space charge is not negligible but in which the voltage drop is sufficiently large to accelerate the ions to a drift energy corresponding to the electron temperature. C+K call it the sheath (p. 45). Its equations are

$$En_+ = J_d$$

$$E^2 \frac{dE}{dn_-} = E - J_d/n_- \tag{abs 1) (Eq. 4, p. 46}$$

This equation has to be solved numerically.

The pre-sheath is joined to the plasma where the two conditions $n_+ < 2n_-$, $J_d < 2J$ are well satisfied. This leads to inequalities

$$\frac{4}{3} n_-^2 < n_o^2 < n_-^3 \tag{abs 2}$$

which can be satisfied by

$$n_- = n_a = n_o^{4/5} \tag{abs 3}$$

but n_o had better be quite large or the overlap region (abs 2) will not be appreciable. For practical plasmas numerical solutions of (ab 2), extending to reasonably large n_o, will be required. Unfortunately there is no approximate solution from which the thickness

of the pre-sheath can be calculated.

(bcs) The Sheath $\tau \to 0$ $n_- \to 0$ $\mu < n_-/n_+ < \sqrt{\mu}$

In the sheath, as generally understood, the electron space charge may be neglected. We shall not, however, neglect the electron flow. The equations are then

$$En_+ = J_d$$

$$\frac{dn_-}{dE} = -\frac{E^2 n_-}{J_d} - \mu E. \tag{bcs 1}$$

The solution of the second is

$$n_- = \mu e^{-V} \int_E^c e^V E \, dE \approx \mu n_{+c} e^{V_c - V}, \tag{bcs 2}$$

where

$$V = E^3/3J_d \tag{Top eq., p. 48}$$

and

$$x_c - x_b = \frac{E_c^2 - E_b^2}{2J_d} = \frac{1.04}{J_d^{1/3}} \left(V_c^{2/3} - V_b^{2/3}\right). \tag{bcs 3}$$

The solution (bcs 2) is joined to the pre-sheath where the conditions of (abs 1) and (bcs 1) overlap, which turns out to include

$$(n_-/n_+)_b = \sqrt{\mu}. \tag{bcs 4}$$

Thus

$$n_b^3 = n_o^3 e^{-3V_b}$$

$$n_{+b}^3 = \frac{J_d^3}{E_b^3} = \frac{J_d^2}{3V_b}$$

$$\frac{n_o}{\mu^{3/2}} = \frac{e^{3V_b}}{3V_b}. \tag{bcs 5}$$

Here, we have taken $J_d^2 = n_o^2$ (a 2) as being close enough.

Similarly,

$$(n_-/n_+)_c = \mu \tag{bcs 6}$$

and

$$\frac{n_o}{\mu^3} = \frac{e^{3V_c}}{3V_c}. \tag{bcs 7}$$

Equations (bcs 5) and (bcs 7) give the potentials of the sheath, and by introducing them in (bcs 3) we can evaluate the sheath thickness. In general,

$$x_c - x_b \approx \frac{V_c^{2/3}}{J_d^{1/3}} \approx \frac{\ln\left(n_o/\mu^3\right)}{3n_o^{1/3}} \tag{bcs 8}$$

but if V_b is large, so that the sheath potential $V_c - V_b$ is small,

$$x_c - x_b \approx \frac{\Delta V^{2/3}}{J_d^{1/3}} \approx \frac{\ln 1/\mu}{\left(9n_o \ln n_o/\mu^3\right)^{1/3}}. \tag{bcs 9}$$

Unfortunately the sheath thickness cannot be compared with the cutoff distance n_a/n_o in (a 8). For small values of V_b one could set $n_a = n_o^{2/3}$, and (bcs 8) shows that the sheath is thicker than the cutoff, but for large V_b there is no suitable value of n_a where the sheath and the plasma overlap. The pre-sheath thickness has to be included.

The boundary condition (bcs 6) that we have chosen corresponds to setting $\mu J = En_-$. It is therefore the point at which the Boltzmann distribution breaks down. It is because we did not go beyond this point that we could use the simpler expression in (bcs 2). It is also the point where conventional sheath theory breaks down, and the usual procedure of setting the random electron current equal to the directed ion flow is equivalent to (bcs 6). There is, however, a skin outside the sheath.

(cds) The Skin $\qquad J = J_d \qquad E = E_d \qquad \delta < n_-/n_+ < \mu$

The skin is an extension of the ion flow transition. The electron density is so small that the electron current cannot be left out of the equations, but the skin is so thin that the electric field may be taken as constant. Eliminating dE between (s 1) and (s 2), we get

$$-dx = \frac{dn_-}{\mu J + En_-} = \frac{\tau\, dn_+}{J - En_+} \tag{cds 1}$$

$$(1+En_-/\mu J)(1-En_+/J)^{\tau} = 1 \tag{cds 2} \text{ (D. 1. 5)}$$

$$E(x_d - x) = \ln(1+En/\mu J).$$

This has the proper limits, written

$$En_- \approx \mu J \qquad En_+ = J \qquad \text{(Eq. 2, p. 36)}$$

$$n_- \to 0 \qquad n_- = \delta n_+, \qquad \text{(cds 3)}$$

the thickness of the skin $\Delta x = n_-/\mu n_o$ is extremely small so that it does not affect the value of ν. For nearly all purposes, the wall can be put at x_c with the boundary condition (bcs 6).

The Characteristic Curve

Integrating the appropriate equations numerically, C+K obtain the characteristic curve shown in Fig. X-4. We show in the same figure the curve obtained by A+R. A+R

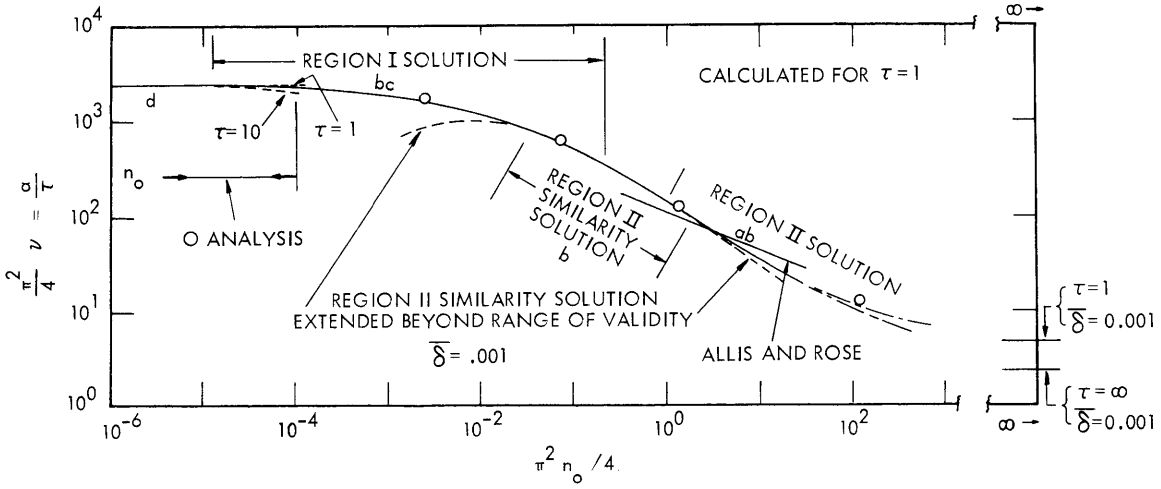

Fig. X-4. Normalized ionization frequency vs plasma density.

used $\mu = 1/32$, C+K used $\mu = 1/1000$. As 1000 is roughly the square of 32, the slope of the C+K curve is roughly twice that of A+R. There is no disagreement. The C+K curve extends farther in both directions because they have dropped the small high derivative term which is most troublesome to a computer, but it does not extend much farther, particularly in the direction of high densities which is of greatest interest. It is for this reason that A+R proposed an approximation, and that C+K in their section D. 3 study the limit $n_o \to \infty$ $n_- \to 0$ and reach the conclusion $\nu \to \nu_a$ from below. As this is surprising, we must look into their analysis of this limit with some care.

(as) The Ambipolar Singularity $\qquad n_o \to \infty \qquad n_- \to 0$

In their section D. 3, C+K consider the singularity created by the somewhat contradictory limits $n_o \to \infty$ $n_- \to 0$. As we have seen, the ambipolar limit is valid only for

$$n_-^3 > n_{ab} = n_o^2 \qquad \text{(as 1)}$$

but since

$$n_{ab}/n_o = n_o^{-1/3} \to 0 \qquad \text{(eq. 4, p. 60)}$$

as

$$n_o \to \infty,$$

the fraction of the plasma where the ambipolar limit is invalid decreases as n_o increases.

The terms on the right of equation (e 11) are small for $n_- > n_{ab}$; hence, we can substitute from (a 2) to get

$$\frac{1+\mu}{1+\tau} J^2 = n_o^2 - n^2 + A n_o \frac{n_o - n}{n} \qquad \text{(as 2) (D. 3. 9)}$$

$$A = \frac{1-\delta}{1+\tau} \frac{1-2\tau-3\delta}{(1+\mu)^2}.$$

We note that the new term is small of order $1/n_o$ compared with the first near the center but large of order $1/n$ near the wall. A recursive procedure will produce converging terms at the center, diverging terms at the wall. Surprisingly, C+K expand (D. 3. 9) in powers of $\xi = (x_d - x)$ about the singularity at $n = 0$ (D. 3. 10). This is dangerous because the series has no validity at its origin.

They now seek a sheath solution, making use of (e 14) which can be written

$$(1+\tau)n_- = a + \frac{E^2}{2} - \tau s + (1+\mu) \int_x^{x_d} J \, dx,$$

where (as 3) (D. 3. 11)

$$a = n_o + \tau n_{+o} - (1+\mu) \int_0^{x_d} J \, dx.$$

The terms of order n cancel in "a", as can be seen by setting

$$J = \sqrt{\nu} \, n_o \sin x/\Gamma_\nu \qquad \text{(as 4)}$$

which yields

$$a = n_o + \tau n_{+o} - (1+\mu)\nu n_o.$$

For ν near its ambipolar value,

$$\nu = \frac{1+\tau}{1+\mu} + \nu_1/n_o \qquad \text{(as 5)}$$

$$a = \tau s_o - (1+\mu)\nu_1. \qquad \text{(as 6)}$$

C+K now expand (as 3) in powers of ξ, which is correct. The solution (as 3) should be joined to (as 2) in the region where both are valid, that is, for $n_- > n_a$. C+K do not do this. On pp. 68 and 69 they equate the power series term by term. This is equivalent to equating the functions and several derivatives at the origin of the series, that is, at n = 0; however, (as 2), their (D. 3. 9), does not even approximate the solution at n = 0. We have carried our approximation (as 4) farther than we should in (as 6) so that this equation can be compared with the third equation on p. 68 of C+K. Following them and neglecting τs_o, one finds that the two equations turn out to be the same but with opposite signs. Recursion procedures often give alternating signs when they diverge.

C+K find different signs for ν_1 in isothermal and active plasmas. The reason for this is seen in the sign of α (a 6) in the distributed charge formula (a 9). α changes sign for $\tau = 1/(2+3\mu)$. This can be traced back to the sign of σ in (e 11) and taking the derivative of the limit formula (a 3) to insert in s'; however, s' is a sharply peaked function in the ambipolar limit and s' changes sign quickly in the pre-sheath. Thus the joining procedure is more difficult in the isothermal case and it would be better to use the first integral (e 13).

W. P. Allis

References

1. I. M. Cohen and M. D. Kruskal, Asymptotic Theory of the Positive Column of a Quiescent, Longitudinally Uniform Gas Discharge, Matt-202, Plasma Physics Laboratory, Princeton University, Princeton, N.J., July 1963.

2. W. P. Allis and D. J. Rose, The transition from free to ambipolar diffusion, Phys. Rev. 93, 84-93 (1964).

B. ION CYCLOTRON RESONANCE IN A RADIOFREQUENCY DISCHARGE

Ion cyclotron resonance has been observed in a rather unique RF discharge. As shown schematically in Fig. X-5, the discharge is produced by a single electrode that is a thermionic electron emitter (oxide-coated). The discharge appears to fill entirely a region, 10 cm in diameter by 20 cm long, formed by electric insulators. The DC magnetic field $\underset{\sim}{B}_o$ is uniform within 1 1/2 per cent over this region. Also indicated in Fig. X-5 are two magnetic pickups; the smaller is enclosed in 8-mm quartz tubing and measures the AC magnetic field that is perpendicular to $\underset{\sim}{B}_o$, the larger is wrapped on the discharge tube and measures the AC magnetic field that is parallel to $\underset{\sim}{B}_o$. Signals from these pickups are detected and then plotted directly as a function of B_o on an

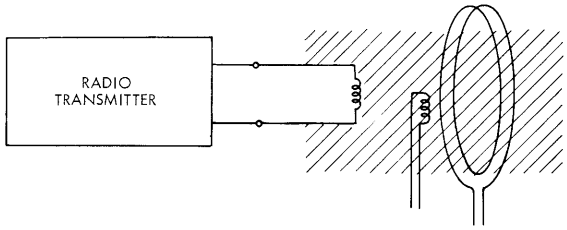

Fig. X-5. Schematic representation of the system.

x-y recorder. The frequency of the applied voltage is constant, and ion cyclotron resonance is expected when

$$\beta_+ = \frac{eB_o}{M_+\omega} = 1.$$

Data obtained in a hydrogen discharge are shown in Figs. X-6 and X-7. The hydrogen pressure is approximately 20 μ, and the applied frequency is 4 Mc. It is assumed that the hydrogen is disassociated and thus β_+ is based on the proton mass. The curves obtained from the two pickups are roughly similar and only those for the smaller one are given here.

In Fig. X-6 the detector is tuned to 4 Mc; in Fig. X-7 it is tuned to 8 Mc. The response of a wideband detector (10 cps to 10 Mc) showed little or no resonance behavior.

The 8-Mc signal is stronger than the 4-Mc signal. In order to get comparable responses in Figs. X-6 and X-7, the 8-Mc signal was attenuated 13 db. The light showed considerable modulation at 8 Mc, little at 4 Mc.

The curves of Figs. X-6 and X-7 are labeled with the applied peak-to-peak voltage. This voltage varies little with B_o. In fact, it is essentially the same for a given setting of the transmitter controls, with or without a plasma. The shapes of the curves depend on the applied voltage. This is thought to be due to variation in the plasma density. A similar dependence on the pressure is observed.

It is tempting to relate peaks observed for $\beta_+ < 1$ to plasma resonance of the extraordinary wave propagating across $\underset{\sim}{B}_o$. The resonance condition for a lossless plasma is

$$\alpha^2 = \frac{\left(\beta_-^2 - 1\right)\left(1 - \beta_+^2\right)}{\beta_-\beta_+ - 1} \approx \frac{M_+}{m_-}\left(1 - \beta_+^2\right),$$

where $\beta_- = e\,B_o/m_-\omega$, and the approximation applies in the vicinity of ion cyclotron resonance. A resonance occurring at $\beta_+ = 0.8$ would, then, correspond to $\alpha = 25.7$, or a plasma density of 1.3×10^8 cm^{-3}.

It is equally tempting to relate peaks observed for $\beta_+ > 1$ to generation of ion cyclotron waves. The dispersion relation for a lossless plasma is

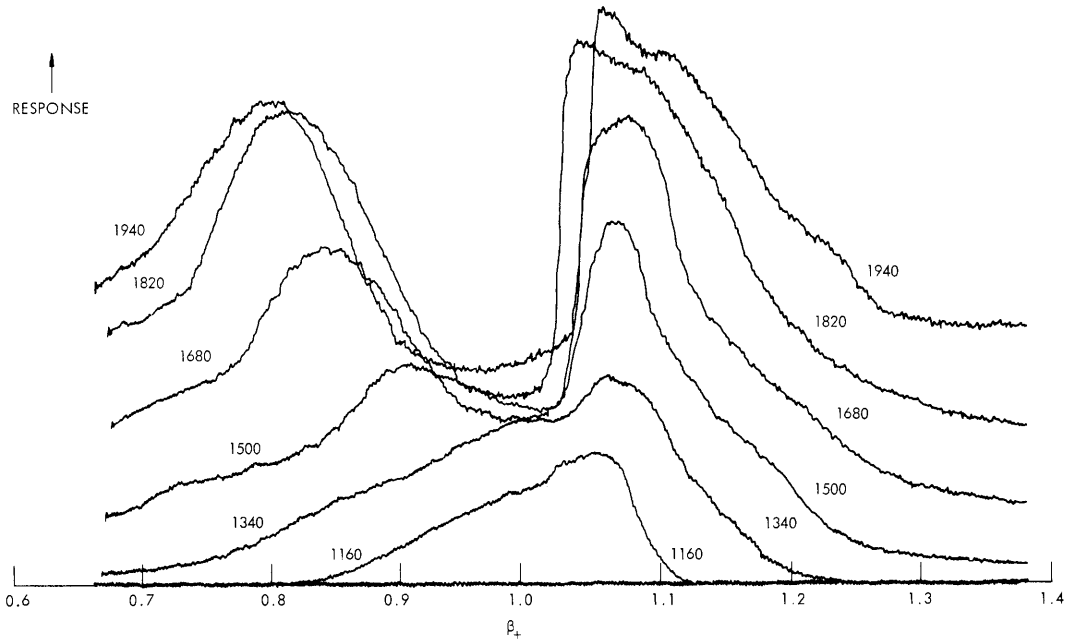

Fig. X-6. Receiver response vs magnetic field, receiver tuned to 4 Mc.

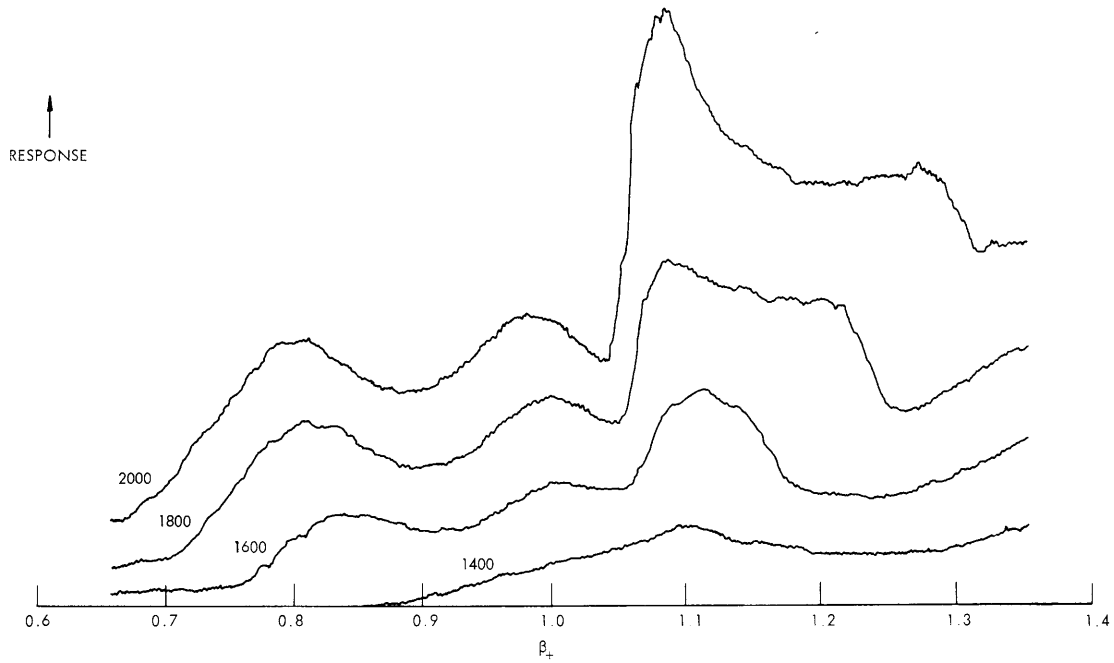

Fig. X-7. Receiver response vs magnetic field, receiver tuned to 8 Mc.

$$n^2 = 1 - \frac{\alpha^2}{(1-\beta_+)(1+\beta_-)} \approx \frac{m_-}{M_+} \frac{\alpha^2}{\beta_+(\beta_+-1)},$$

for which the approximation again applies in the vicinity of ion cyclotron resonance. If we take the 20-cm length as approximately $\lambda/4$, $n \times 100$, since the free-space wavelength is 75 meters. The loading at $\beta_+ = 1.1$ would then correspond to $\alpha = 1.4 \times 10^3$, or a plasma density of 4×10^{11} cm^{-3}.

If both resonances are observed the plasma resonance must occur in the outer regions of the plasma. The existence of the plasma resonance has not yet been verified. Distinct peaks, however, have occasionally been observed at $\beta_+ = 1$ and $\beta_+ > 1$. The second peak then grows, relative to the first, and moves to higher β_+ as the applied voltage or pressure is increased. This gives some support to the ion cyclotron wave interpretation.

J. J. Nolan, Jr.

C. ELECTRON CYCLOTRON ABSORPTION IN THE CESIUM AFTERGLOW

A knowledge of the electron-atom collision frequency in cesium as a function of electron velocity is essential in order to calculate transport coefficients in the thermionic energy converter, which uses cesium plasma as the conducting medium.

Many experimental measurements[1] have been made of this quantity, no two agreeing entirely. The disagreement arises from the limited range of electron energies over which the data were valid, the uncertainty of the electron energy, and the differences in the techniques of measurement. Recently Stone and Reitz[2] have given a theory for the collision cross section of slow electrons with cesium atoms. The experimental data is rather widely scattered about their theoretical curve.

In order to obtain a set of data connecting the limited regions of experimentation of other workers, an experiment has been devised in which the electron-atom collision frequency can be measured over a wider range of electron energies. Preliminary measurements have been made. The wide range of energies is obtained from the afterglow period of a pulsed DC discharge in cesium. During this period the electron temperature decays from about 5000°K to 500°K. By using the transient microwave radiometer,[3] it is possible to sample radiation emitted by and transmitted through the plasma during a short interval of time (1, 20, 200 or 1000 μsec). The choice of a certain time in the afterglow at which to sample fixes an electron temperature, which may be measured by using the radiometer technique. Then by employing a highly attenuated klystron probing signal of magnitude only one hundred times that of the thermal radiation from the plasma (so that the probing signal does not heat the plasma), the transmission of the plasma is measured at this temperature with the radiometer now used as a detector for the klystron

signal. The klystron signal is propagated through the plasma in a direction parallel to a DC magnetic field that is applied to the plasma in such a way that when the signal electric field is of the proper frequency it will interact strongly with the plasma electrons as they orbit in the magnetic field. The transmission of the plasma is then measured as a function of the magnetic field and the width of this cyclotron resonance can be related

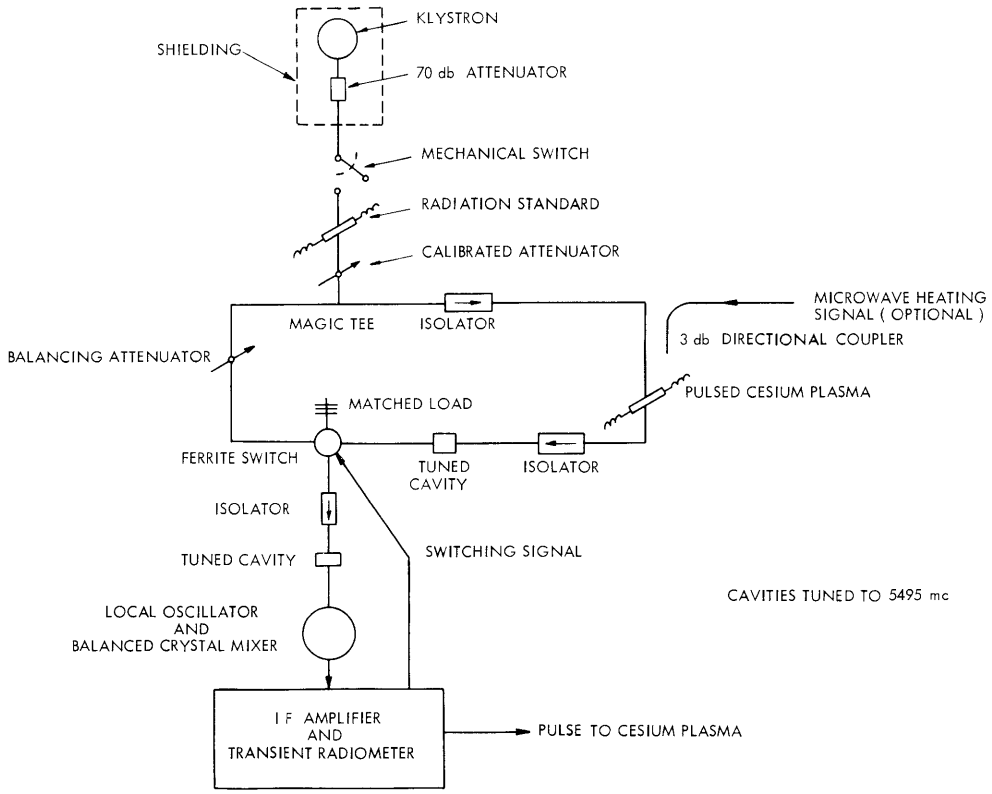

Fig. X-8. Microwave circuit for transient absorption and temperature measurements.

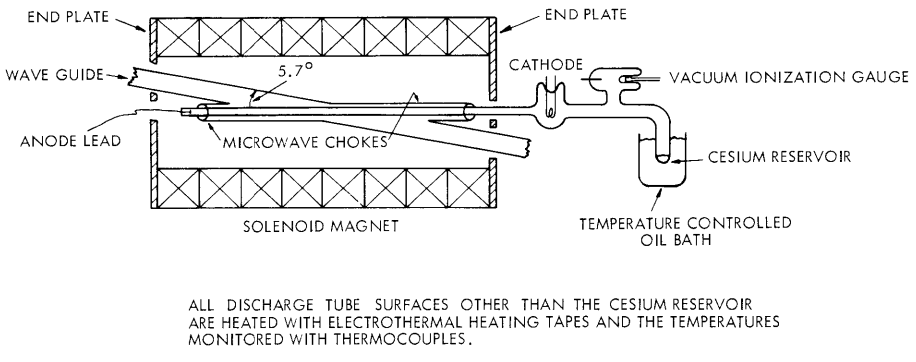

Fig. X-9. Cesium quartz discharge tube and magnetic field configuration.

to the electron-atom collisions which interrupt the motion of the orbiting electrons.

1. Experimental Arrangement

Figure X-8 shows the microwave bridge circuit that is used to measure transient temperatures and plasma absorption. The details of the temperature measurement have been described in previous reports.[3] When absorption measurements are to be made, the radiation standard is turned off, the klystron at the top of the figure is switched on, and the plasma absorption in the right arm of the bridge is balanced with the attenuator in the left arm.

The cesium plasma is contained in a 1.3×75 cm cylindrical quartz discharge tube that is inserted at an angle of $5.7°$ through the broad face of a 1×2 inch rectangular brass waveguide (See Fig. X-9). Microwave chokes prevent radiation leakage from the waveguide. A pulsed DC discharge is used to produce the plasma; the currents and voltages are about 20 ma and 200 v at a cesium pressure of 0.03 torr. The cesium pressure is determined by the vapor pressure of cesium vapor in equilibrium with a cesium puddle in a reservoir whose temperature is carefully controlled by an oil bath. The rest of the tube is maintained ~50°C hotter than the reservoir by using electrothermal heating tapes and thermocouples to monitor the temperature.

2. Theory

The absorption coefficient of a tenuous, waveguide-contained plasma that is longitudinally magnetized may be calculated by using a perturbation theory in which the unperturbed electromagnetic field is given by the modes of the empty waveguide. The general equations have been given by Bers[4]; the result of the perturbation calculation for α, the power absorption coefficient, is

$$\alpha = -\frac{\left(\frac{1}{10}\right)\omega_{p_o}^2}{2c\sqrt{1-\left(\frac{\lambda}{2a}\right)^2}}\left(-\frac{4\pi}{3}\int_0^\infty\left(\frac{\nu_c}{(\omega-\omega_b)^2+\nu_c^2}+\frac{\nu_c}{(\omega+\omega_b)^2+\nu_c^2}\right)\frac{df^o}{dv}v^3\,dv\right), \tag{1}$$

where

$\omega_{p_o}^2 = \frac{n_o e^2}{m\epsilon_o}$, the square of the electron plasma frequency

c = velocity of light

$\omega_b = \frac{eB}{m}$, the electron cyclotron frequency

ν_c = electron-atom collision frequency

$\omega = \frac{2\pi c}{\lambda}$, radian frequency of the probing wave

v = electron speed

f^o = electron velocity distribution in absence of the probing signal

n_o = electron density at the center of the discharge tube

a = the wider dimension of the rectangular waveguide.

The factor of 1/10 corrects for the fact that the plasma fills only the center portion of the waveguide cross section. The electron density is assumed to be distributed in the fundamental diffusion mode across the discharge tube cross section, and the magnetic field is assumed parallel to the waveguide axis.

The perturbation calculation is only valid provided the plasma index of refraction does not deviate significantly from one.

A more detailed calculation of α and of the plasma emission coefficient is in progress.

When the plasma electrons have a Maxwellian distribution of velocities $\frac{df^o}{dv} = -\frac{mv}{kT} f^o$, and the magnetic fields are near cyclotron resonance, α may be written as

$$\alpha = -\frac{\left(\frac{1}{10}\right)\omega_{p_o}^2}{2c\sqrt{1-\left(\frac{\lambda}{2a}\right)^2}}\left(\frac{4\pi m}{3kT}\int_0^\infty \frac{v^4 f^o \nu_c}{\nu_c^2 + (\omega-\omega_b)^2}\right)dv \qquad (2)$$

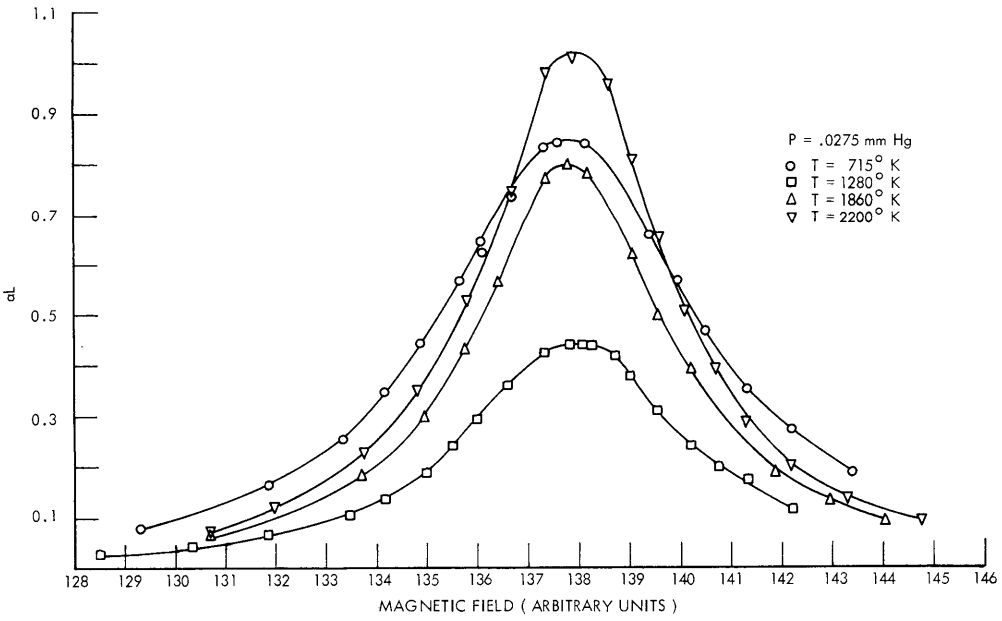

Fig. X-10. Dependence of plasma absorption (αL) on magnetic field for various electron temperatures at a pressure of 0.0275 torr.

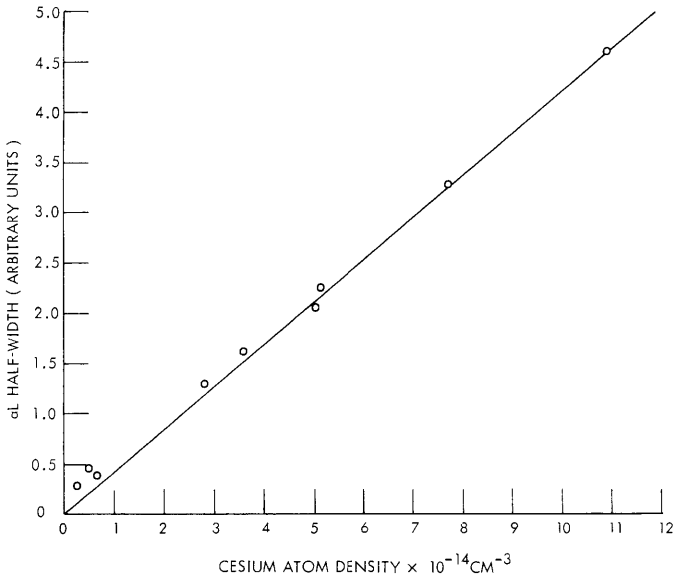

Fig. X-11. Half-width of αL versus cesium atom density.

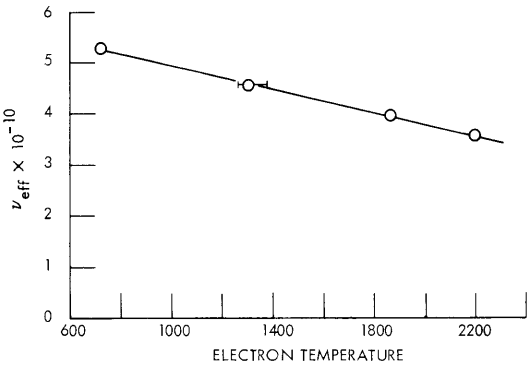

Fig. X-12. Effective collision frequency, calculated from half-widths of Fig. X-10, versus electron temperature.

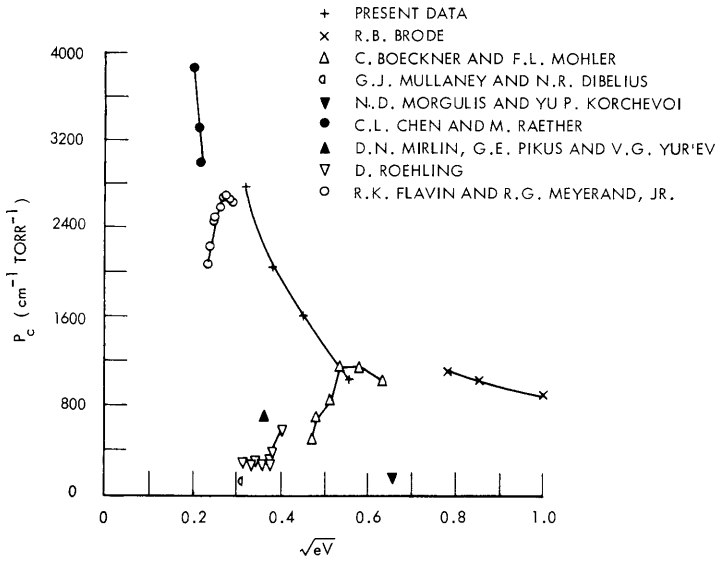

Fig. X-13. P_c for cesium, determined by various experimenters.

The experimental study is based on the measurement of α as a function of ω_b. From a knowledge of the Maxwellian nature of f^o, the measured electron temperature, and the shape of the resonance of α, it is possible to determine the velocity dependence of ν_c.

3. Experimental Results

Preliminary measurements of the dependence of α on the magnetic field have been made for several different cesium atom densities corresponding to pressures up to 0.059 torr at an electron temperature of 2200°K; similar measurements have been made for various electron temperatures at a pressure of 0.0275 torr.

Figure X-10 gives the data taken at fixed pressure and shows αL ($L \approx 20$ cm is the effective length of the discharge tube in the waveguide) as a function of magnetic field. The change in the shape of the resonance with temperature reflects a change in the velocity dependence of ν_c. Figure X-11 shows the results at fixed temperature, and the half-width of αL is plotted versus cesium atom density. At higher pressures the half-width is linear with density. The nonlinearity at low densities is caused by magnetic field inhomogeneities and by Doppler broadening resulting from electron thermal motion along the magnetic field lines.

An effective collision frequency ν_{eff} may be calculated from the half-width expressed in units of frequency and plotted against electron temperature to gain a qualitative feeling for the energy dependence of the real collision frequency. This effective collision frequency, evaluated for a density of cesium atoms corresponding to 1 torr and 273°K, is plotted in Fig. X-12 and shows a tendency to decrease with increasing temperature.

To make a satisfactory comparison with other experiments, the correct velocity dependence of ν_c must be determined by assuming a polynomial velocity dependence of ν_c, fitting the resonance curves of Fig. X-10, and then calculating the collision probability $P_c = \nu_c/v$. We can, however, calculate $P_{eff} = \nu_{eff}/(\overline{v^2})^{1/2}$ and compare this with other experimental data. $P_{eff} = P_c$ only when ν_c is independent of electron velocity. The results of this approximation are plotted along with the experimental results of others in Fig. X-13. If a more quantitative analysis of the data were made, stronger conclusions might be drawn. At present, the great variation in the experimental data serves as a stimulus to further work.

Three other points are worth mentioning at this time. For all measurements of this experiment the electron velocity distribution was ascertained to be Maxwellian by checking that the measured electron temperature showed no resonance at cyclotron frequency.[5] This required operating at peak values of αL as large as one (see Fig. X-10). The condition that the plasma index of refraction be ~1 for all values of ω_b is satisfied provided that $\frac{\omega_p^2}{2\omega_b \nu_c} \ll 1$. For a velocity-independent ν_c, if we use Eq. 2, $(\alpha L)_{max} \approx \frac{L}{20c} \frac{\omega_p^2}{\nu_c}$,

so that the condition may be written as

$$\frac{\omega_p^2}{2\omega_b \nu_c} = \frac{(\alpha L)_{max}\, 20c}{L\, 2\omega_b} = (\alpha L)_{max}\left(\frac{10\lambda}{2\pi L}\right) \ll 1. \tag{3}$$

But $\lambda = 6$ cm and $L = 20$ so that for $(\alpha L)_{max} = 1$, this quantity is ~1/2. In spite of this, no change in the symmetry of the lines was found for the large values of αL.

The third point is that a microwave heating field will be employed to widen the spectrum of available electron temperatures in the afterglow. The experimental provision made for this is shown in Fig. X-8.

J. C. Ingraham

References

1. R. B. Brode, Phys. Rev. 34, 673 (1929); C. Boeckner and F. L. Mohler, Bur. Std. J. Res. 10, 357 (1933); G. J. Mullaney and N. R. Dibelius, Am. Rocket Soc. J. 31, 1575 (1961); N. D. Morgulis and Yu. P. Korchevoi, Zh. Tekhn. Fiz. (English transl.: Soviet Phys. – Tech. Phys.), Vol. 32, No. 7, pp. 900-902 (1962); C. L. Chen and M. Raether, Phys. Rev. 128, 2679 (1962); D. N. Mirlin, G. E. Pikus, and V. G. Yurév, Soviet Phys. – Tech. Phys. 7, 559 (1962); D. Roehling, Symposium on Thermionic Power Conversion, Los Alamos Scientific Laboratory, May 1962; R. K. Flavin and R. G. Meyerand, Advanced Energy Conversion (Pergamon Press, New York, 1963), Vol. 3, pp. 3-18.

2. P. M. Stone and J. R. Reitz, Elastic scattering of slow electrons by cesium atoms, Phys. Rev. 131, 2101 (1963).

3. J. C. Ingraham and J. J. McCarthy, Quarterly Progress Report No. 64, Research Laboratory of Electronics, M.I.T., January 15, 1962, p. 76; J. C. Ingraham, Quarterly Progress Report No. 66, Research Laboratory of Electronics, M.I.T., July 15, 1962, p. 83.

4. A. Bers in W. P. Allis, S. J. Buchsbaum, and A. Bers, Waves in Anisotropic Plasmas, (The M.I.T. Press, Cambridge, Mass., 1963), p. 136.

5. H. Fields, G. Bekefi, and S. C. Brown, Phys. Rev. 129, 506 (1963).

D. RADIOFREQUENCY CYCLOTRON CONFINEMENT

Work has been extended on the theory of RF confinement at exact ion cyclotron resonance, discussed by Whitehouse,[1] Kulinski,[2] and others. Their theories do not explicitly treat the way the plasma modifies the fields. The present work has made it possible to estimate the penetration of an RF field into a plasma in the geometry discussed by Whitehouse, and then to compute the modifications to the RF confinement.

A two-dimensional geometry is used to make the problem tractable. (See Fig. X-14.) The conductor is excited antisymmetrically by the surface current J, which produces a

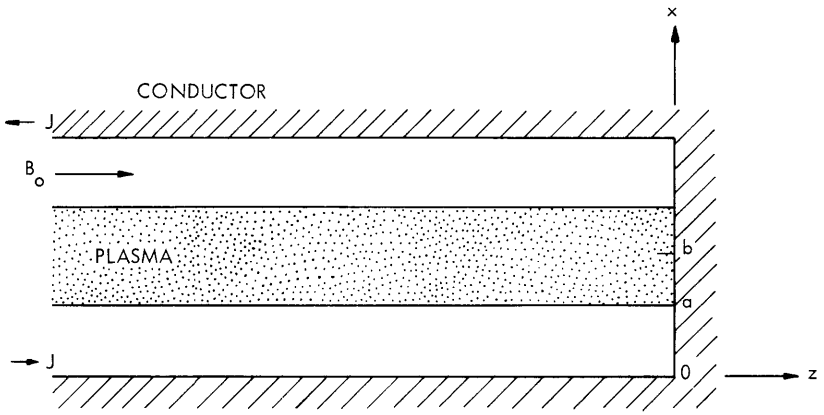

Fig. X-14. Cross section of plasma slab and conductor.

magnetic field H_y out of the paper. The problem is to determine the penetration of the magnetic field into the plasma whose dielectric constant may be extremely large. We assume a diagonal form of the dielectric tensor but allow $K_\perp$ to be different from $K_\parallel$. This problem would be very combersome if handled in terms of the standard E_z modes but becomes very simple if handled in terms of H_y modes. Using Maxwell's equations we then arrive at the following equations

$$-\frac{\partial H_y}{\partial z} = i\omega\epsilon_o K_\perp E_x \tag{1a}$$

$$\frac{\partial H_y}{\partial x} = i\omega\epsilon_o K_\parallel E_z \tag{1b}$$

$$\frac{1}{K_\perp}\frac{\partial^2 H_y}{\partial z^2} + \frac{1}{K_\parallel}\frac{\partial^2 H_y}{\partial x^2} + \frac{\omega^2}{c^2} H_y = 0, \tag{2}$$

where the first two will be used to find E_x and E_z once H_y is known. We assume an H_y of the form

$$H_y = H\, e^{ikz+i\omega t} \times \begin{cases} e^{i\beta x} & \text{inside the plasma} \\ e^{-\delta x} & \text{outside the plasma} \end{cases}$$

Using the boundary conditions and the antisymmetric excitation we arrive at the determinantal equation.

$$\delta \tanh \delta a = \frac{\beta}{K_\parallel} \tan \beta(b-a) \tag{3}$$

This equation determines k since both δ and β are functions of k and ω by (2). If we now assume that $\beta(b-a) \ll \frac{\pi}{2}$, we can expand the tangents on either side of (3) and arrive at an approximate equation for k,

$$k \approx \frac{\omega}{c}\frac{b}{a}. \tag{4}$$

The condition for validity of Eq. 4 can be expressed in another form

$$\frac{\omega_p}{c}(b-a) \ll \frac{\pi}{2}. \tag{5}$$

This approximate value for k will be useful for interpreting the general field solution inside the plasma. For $b \leq x \leq a$,

$$H_y = J \cosh \delta a \left[\cos\beta(x-a) + \tan\beta(b-a)\sin\beta(x-a)\right]\cos kz \tag{6a}$$

$$E_z = -\frac{\beta}{K_{||}}\frac{J \cosh \delta a}{i\omega\epsilon_o}\left[\sin\beta(x-a) - \tan\beta(b-a)\cos\beta(x-a)\right]\cos kz \tag{6b}$$

$$E_x = \frac{kj \cosh \delta a}{i\omega\epsilon_o K_\perp}\left[\cos\beta(x-a) + \tan\beta(b-a)\sin\beta(x-a)\right]\sin kz \tag{6c}$$

It is clear that H_y and E_x are symmetric about the line $x = b$, while E_z is antisymmetric about this line. These equations coupled with the approximate determinantal equation now answer the question whether or not H_y penetrates into the plasma slab. Even though a large $K_\perp$ may shield the plasma from E_x, the magnetic field H_y will penetrate if $\beta(b-a)$ is considerably less than $\frac{\pi}{2}$. From (6b) it can be seen that β is associated with an E_z field. Since this field is parallel to the plasma boundary, it cannot be shielded out by the plasma. It is the E_z field that allows the magnetic field to penetrate the plasma.

Returning now to the problem of the particle's orbit treated by Whitehouse, we use Eq. 6a and 6c in the limit $\beta(b-a) \to 0$ to specify the H_y and E_x. This assumes a thin slab of plasma. Using these fields we derive the following equation for the z velocity of a particle

$$\dddot{z} + \left[\Omega_\perp^2 + (\omega \mp \Omega_z)^2\right]\ddot{z} + \frac{\omega(\omega \mp \Omega_z)\,\Omega_\perp^2}{K_\perp} z = 0, \tag{7}$$

which differs from Whitehouse's Eq. 7 only by the presence of $K_\perp$. At resonance the equation for the z motion is the same, giving identical z reflection. However, the transverse energy that a reflected particle picks up during reflection will be quite different from that computed by Kulinski for reflection in a plane wave. He finds[3] that the ratio of the transverse energy, at the point where the particle's Z motion just stops,

to its initial z energy is approximately $4\left(\frac{B_o}{B_{RF}}\right)^2$. For typical values of B_o and B_{RF}, this ratio can be extremely large and puts a severe restriction on the design of a simple experiment. Our theory indicates that E_x will be approximately $\frac{1}{K_\perp}$ times the free space E_x that Kulinski considers, and therefore a particle can be reflected without an extreme increase in its transverse energy.

P. W. Jameson

References

1. Quarterly Progress Report No. 73, Research Laboratory of Electronics, M. I. T., April 15, 1964, p. 40.

2. S. Kulinski, Rijnhuizen Report 63-14, FOM-Instituut Voor Plasma-Fysica, Jutphass, Netherlands, November, 1963.

3. S. Kulinski, Ibid., p. 19, Eq. 66.

E. DEFINITION OF THE "RAY REFRACTIVE INDEX" AND ITS ROLE IN THE RADIATION IN ANISOTROPIC PLASMAS

Studies of the flow of radiation in inhomogeneous, dispersive media are based on a classical theorem of geometrical optics by Clausius. This theorem can be stated as follows: Consider two points O_1 and O_2 of the medium (Fig. X-15), lying within elementary areas da_1 and da_2, respectively. Let R be the distance between O_1 and O_2 and let the

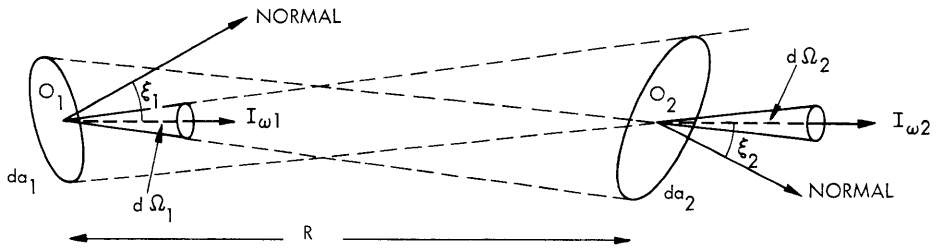

Fig. X-15. Rays between two points, O_1 and O_2, at which the respective intensities of radiation are $I_{\omega 1}$ and $I_{\omega 2}$.

normal to da_1 make an angle ξ_1 with O_1O_2, and the normal to da_2 make an angle ξ_2 with O_1O_2. The distance R is taken to be large compared with da_1 and da_2 so that all pencils of radiation passing through a point of da_1 and filling da_2 have essentially the same solid angle $d\Omega_1$; similarly, $d\Omega_2$ is the solid angle of every pencil of rays passing da_2 and filling area da_1. Then if n_1 and n_2 are the refractive indices at O_1 and O_2, as a consequence of Snell's law of refraction,

$$n_1^2 \cos \xi_1 \, da_1 d\Omega_1 = n_2^2 \cos \xi_2 \, da_2 d\Omega_2,$$

or

$$n^2 \cos \xi \, da d\Omega = \text{constant along the ray.} \tag{1}$$

This is Clausius's theorem. The theorem is not valid, however, in anisotropic dispersive media. Nevertheless, one may write

$$n_r^2 \cos \xi \, da d\Omega = \text{constant along the ray.} \tag{2}$$

Here, the quantity n_r plays the role of n in isotropic materials. For lack of better terminology, we call n_r the "ray refractive index."

It is found that n_r is related to n and to the magnitude of the group velocity w through

$$n_r^2 = \left| n^2 \frac{w}{c} \frac{d\Omega_k}{d\Omega} \left(\frac{\partial \omega n}{\partial \omega} \right)_{\theta, \phi} \right|, \tag{3}$$

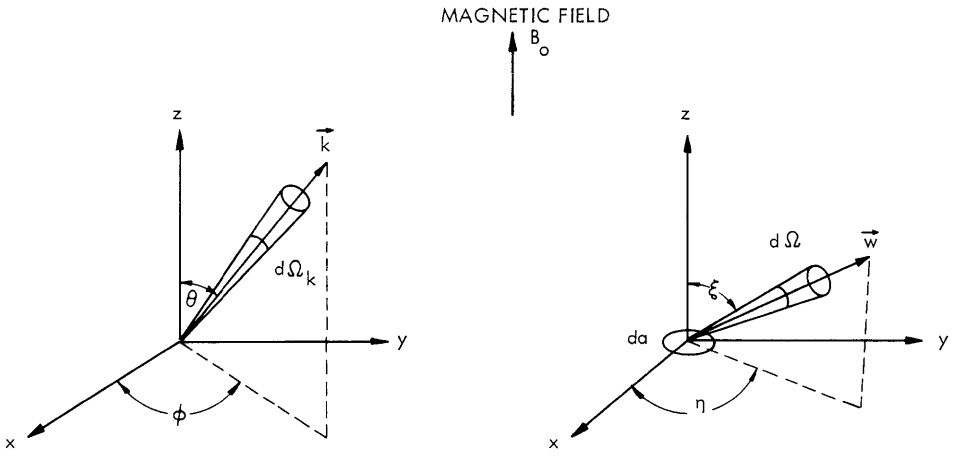

Fig. X-16. Direction of wave vector $\vec{k}$ and of group velocity vector $\vec{w}$, at a point in the medium. The elementary area, da, across which the flux of radiation is considered, is taken to lie in the xy plane.

where $d\Omega = \sin\xi\, d\xi d\eta$ is the elementary solid angle about the ray direction, and $d\Omega_k = \sin\theta\, d\theta d\phi$ is the elementary solid angle about the wave-vector direction with which the bundle of rays is associated. (See Fig. X-16.) There is a set of equations like (2) and (3) at a point r of the medium for every independent solution (that is, characteristic mode) of the dispersion equation

$$\omega = \omega(\vec{k}, \vec{r}). \tag{4}$$

Note that n_r is zero for all ray directions associated with angles θ and ϕ for which $k(\theta,\phi)$ is imaginary.

In the case of a plasma immersed in a magnetic field B_o, n is independent of the azimuthal angle ϕ, if the direction of B_o is chosen as the z axis of the polar coordinates z, θ, ϕ. One then finds that

$$\tan(\xi-\theta) = -\frac{1}{n}\left(\frac{\partial n}{\partial\theta}\right)_\omega$$

$$w = \frac{c}{\left(\frac{\partial\omega n}{\partial\omega}\right)_\theta}\left[1 + \left(\frac{1}{n}\frac{\partial n}{\partial\theta}\right)^2_\omega\right]^{1/2} \tag{5}$$

and

$$d\Omega = -\frac{d\Omega_k}{\sin\theta}\frac{\partial}{\partial\theta}\left\{\frac{n\cos\theta + \left(\frac{\partial n}{\partial\theta}\right)_\omega \sin\theta}{\left[n^2 + \left(\frac{\partial n}{\partial\theta}\right)^2_\omega\right]^{1/2}}\right\} \tag{6}$$

with the result that (3) becomes

$$n_r^2 = \left| n^2 \sin\theta \; \frac{\left[1 + \left(\frac{1}{n}\frac{\partial n}{\partial \theta}\right)_\omega^2\right]^{1/2}}{\frac{\partial}{\partial\theta}\left\{\frac{\cos\theta + \left(\frac{1}{n}\frac{\partial n}{\partial\theta}\right)_\omega \sin\theta}{\left[1 + \left(\frac{1}{n}\frac{\partial n}{\partial\theta}\right)_\omega^2\right]^{1/2}}\right\}} \right| . \tag{7}$$

This formula holds both for electromagnetic and longitudinal (electrostatic) waves. When the medium is isotropic, n_r reduces to n.

The "ray refractive index" appears, often in disguised form, in the work of many authors[1-4] (in particular, Rytov and Mercier) who have engaged in the study of thermal and nonthermal radiation in plasmas and other anisotropic media. Before examining n_r in more detail, we summarize some of the more important results.

The results are all based on the following assumptions. The scale length over which n varies appreciably must be large compared with the wavelength in the medium. Thus (i) waves can be considered locally as plane waves satisfying the dispersion equation (4); (ii) the characteristic modes of propagation are not coupled to one another; and (iii) there are no waves reflected at gradients of n.

If there is any damping of the waves in the medium (k complex), then this damping must be very weak. This allows one to neglect damping in calculating ray trajectories and in deriving equations like Eqs. 2-7. It also allows one to define unambiguously quantities like group velocity and energy density of radiation.

1. Equations of Transport of Radiation

In a perfect dielectric which does not emit, absorb, or scatter radiation, the specific intensity I_ω obeys the equation

$$\frac{I_\omega}{n_r^2} = \text{constant along ray}, \tag{8}$$

where I_ω is the energy crossing a unit area per second per unit solid angle per unit radian frequency interval for the characteristic mode in question. Equation 8 is derived from the equations of energy conservation and by application of Eq. 2.

For a medium which both emits and absorbs,

$$n_r^2 \frac{d}{ds}\left(\frac{I_\omega}{n_r^2}\right) = j_\omega - \alpha_\omega I_\omega, \tag{9}$$

where j_ω and α_ω are the emission and absorption coefficients, respectively, and ds is an element of length along the ray direction. The coefficient α_ω can be determined from the dispersion equation (4) and from Eq. 5 through

$$\alpha_\omega = (-2 \text{ Im } k) \cos(\xi-\theta). \tag{10}$$

2. Black-Body Radiation

a. Energy Density

The spectral energy density of black-body radiation for each characteristic mode in an anisotropic medium is given by

$$u_\omega = \frac{u_{o\omega}}{4\pi} \int_{\Omega_k} n^2 \left| \frac{\partial \omega n}{\partial \omega} \right|_\theta d\Omega_k$$

$$= \frac{u_{o\omega}}{4\pi} \int_\Omega \frac{c}{w} n_r^2 d\Omega, \tag{11}$$

where $u_{o\omega}$, the energy density in vacuum (for one polarization), is

$$u_{o\omega} = \frac{\hbar\omega^3}{2\pi^2 c^3} \left[e^{\hbar\omega/\kappa T} - 1 \right]^{-1}, \tag{12}$$

b. Intensity

Since in general u_ω and I_ω are related through

$$u_\omega = \int_\Omega \frac{I_\omega}{w} d\Omega, \tag{13}$$

it follows from (3), (5), (6), and (11) that the black-body intensity, denoted by B_ω, is

$$B_\omega = n_r^2 B_{o\omega}, \tag{14}$$

where $B_{o\omega}$, the black-body intensity in vacuum (for one polarization), is

$$B_{o\omega} = \frac{\hbar\omega^3}{8\pi^3 c^2} \left[e^{\hbar\omega/\kappa T} - 1 \right]^{-1}. \tag{15}$$

c. Kirchhoff's Law

In thermal equilibrium, Kirchhoff's law relates j_ω, α_ω, and $B_{o\omega}$ through

$$\frac{j_\omega}{\alpha_\omega} = n_r^2 B_{o\omega}. \tag{16}$$

When thermal equilibrium does not exist, j_ω and α_ω may be determined separately in terms of the particle momentum distribution functions $f(\vec{p})$ and $f(\vec{p}')$, where $\vec{p}$ and $\vec{p}'$ refer to the two states that participate in the emission of a quantum $\hbar\omega$. Thus

$$j_\omega = \int \eta_\omega(\vec{p'})\, f(\vec{p'})\, d^3p'$$

$$\alpha_\omega = \int \eta_{\omega A}(\vec{p})\, f(\vec{p})\, d^3p - \int \eta_{\omega S}(\vec{p'})\, f(\vec{p'})\, d^3p', \tag{17}$$

where η_ω, $\eta_{\omega A}$ and $\eta_{\omega S}$ are the differential coefficients for spontaneous emission, absorption, and stimulated emission, respectively, and are related (much as Einstein's A and B coefficients) through

$$\eta_\omega(\vec{p'}) = n_r^2 \frac{\hbar\omega^3}{8\pi^3 c^2}\, \eta_{\omega S}(\vec{p'})$$

$$\eta_{\omega A}(\vec{p})\, d^3p = \eta_{\omega S}(\vec{p'})\, d^3p'. \tag{18}$$

Individually, these coefficients have the property that

$$\eta_\omega \propto \frac{c}{w} n_r^2$$

$$\eta_{\omega A} \propto \frac{c}{w} \tag{19}$$

$$\eta_{\omega S} \propto \frac{c}{w}.$$

3. Polar Diagrams of $(1/n)$ and $(1/n_r)$

Several geometrical representations are used in describing wave propagation in an anisotropic medium. One such representation is in terms of the "phase velocity surface," which is a polar plot of the phase velocity

$$\vec{v} = \frac{\omega}{k^2}\vec{k} = c\frac{\vec{n}}{n^2} \tag{20}$$

as a function of the angle θ. From Eq. 20, this is equivalent (except for a constant of proportionality) to a polar plot of $(1/n)$. Much use of such diagrams has been made by Allis, Buchsbaum, and Bers[5] in classifying waves in anisotropic plasmas. In the spirit of this classification one may also inquire into the behavior of the ray refractive index and thus obtain information about the angular distribution of radiant energy. (See, for example, Eqs. 8 and 14.) Figure X-17 shows polar plots of $(1/n)$, which are the same as those of Allis, and polar plots of $(1/n_r)$. The results were derived from the computations by Rytov.[1] They apply to the case of a cold plasma, (thermal motion of electrons is neglected) with stationary ions.

Figure X-18 shows the location of the polar diagrams in relation to a Cartesian plot of the variables $\beta^2 = (\omega_c/\omega)^2$ versus $\alpha^2 = (\omega_p/\omega)^2$, where ω_c and ω_p are the electron

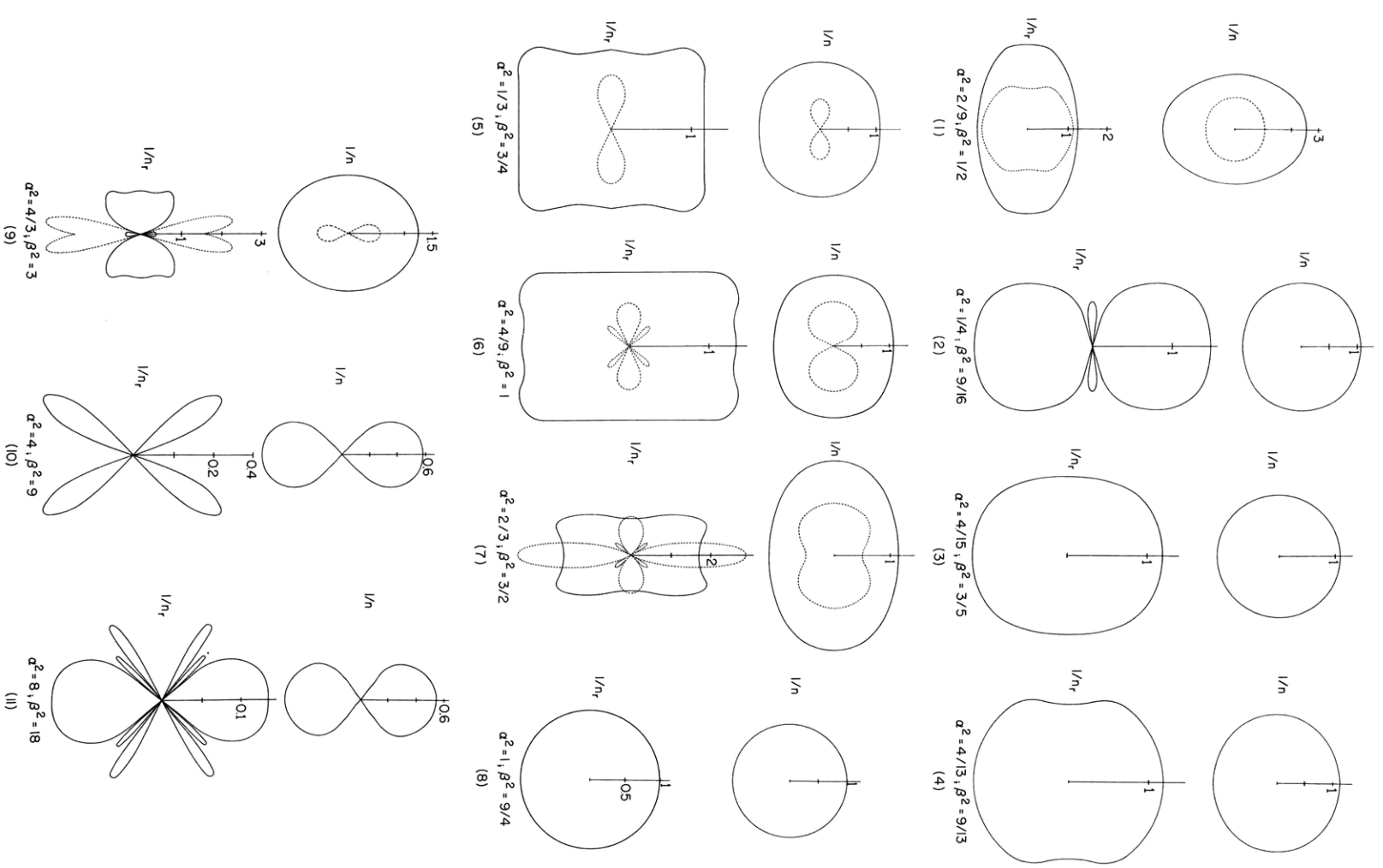

Fig. X-17. Polar plots of $1/n(\theta)$ and $1/n_r(\theta)$. The magnetic field points up (↑) the page. The plots are to scale. The diagrams having solid lines refer to the faster of the two electromagnetic waves. Numbering of the figures (1 to 11) corresponds to the numbering in Fig. X-18. In (8), n_r is the same for both waves; but n is zero for one and unity for the other wave.

cyclotron and plasma frequencies, respectively. We note that all polar diagrams of Fig. X-17 lie on a diagonal passing through the origin of Fig. X-18. This describes a

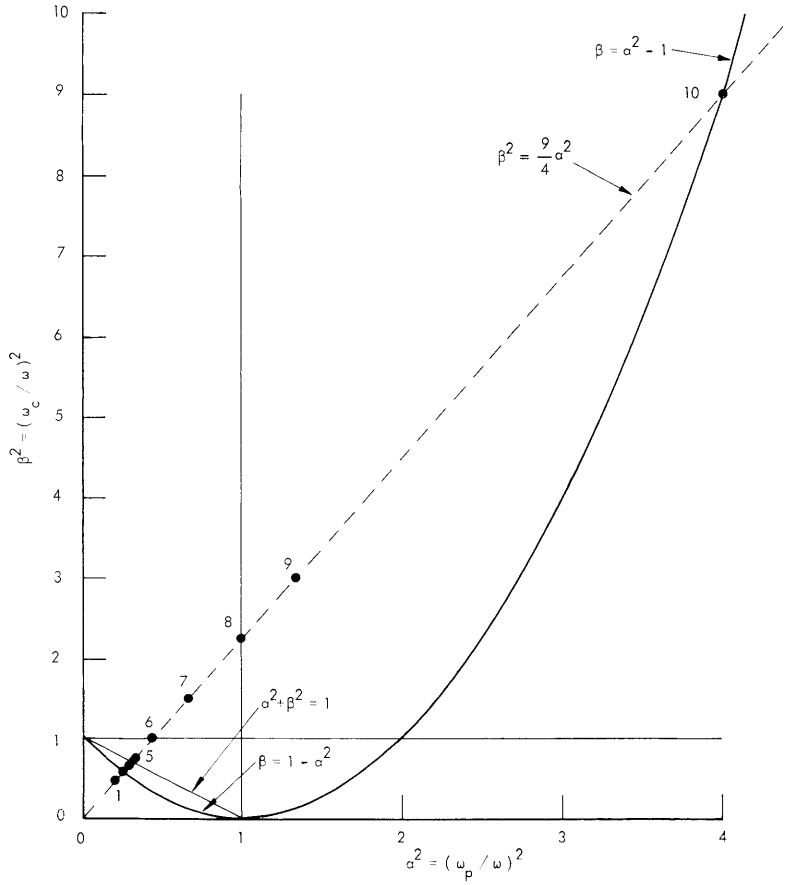

Fig. X-18. The points numbered 1, 2, 3 ... 10 refer to the location in the α^2-β^2 plane of the polar plots shown in Fig. X-17. Polar plot 11 is outside the range of this figure. The significance of all the other straight lines and curves has been discussed by Allis, Buchsbaum, and Bers.[5]

physical situation in which the plasma properties ω_p and ω_c are held fixed and the frequency of observation ω is varied from low frequencies (upper right) to high frequencies (lower left) of Fig. X-18.

For each value of (α^2, β^2) there are two polar plots of $(1/n)$ and $(1/n_r)$. They refer to the two independent electromagnetic waves, called the ordinary and extraordinary in ionospheric studies, and denoted below by superscripts (1) and (2).

For a given direction of wave propagation, the magnitude of n_r^2 is proportional to the radiation intensity. Also, the relative magnitudes of n_r^2 for the two waves is a measure of the degree of polarization of the radiation. Define

$$\text{Degree of polarization} = \frac{I_\omega^{(1)}(\theta) - I_\omega^{(2)}(\theta)}{I_\omega^{(1)}(\theta) + I_\omega^{(2)}(\theta)};$$

then if follows from (8) or (14) that

$$\text{Degree of polarization} = \frac{\left[n_r^{(1)}(\theta)^2 - n_r^{(2)}(\theta)\right]^2}{\left[n_r^{(1)}(\theta)^2 + n_r^{(2)}(\theta)\right]^2}.$$

G. Bekefi

References

1. S. M. Rytov, Theory of Electric Fluctuations and Thermal Radiation, P. N. Lebedev Physical Institute, USSR Academy of Sciences (Academy of Sciences Press, Moscow, 1953). (English Translation, Report AFCRC-TR-59-162, Air Force Cambridge Research Center, Bedford, Mass.).

2. F. V. Bunkin, Soviet Phys.–JETP 5, 665 (1957).

3. R. P. Mercier and H. M. Wills, Physics Laboratory, University of Bristol (unpublished report, 1962).

4. V. I. Pakhomov, V. F. Aleksin, and K. N. Stepanov, Soviet Phys.–Tech. Phys. 6 856 (1962).

5. W. P. Allis, S. J. Buchsbaum, and A. Bers, Waves in Anisotropic Plasmas (The M.I.T. Press, Cambridge, Mass., 1963).

F. APPLICATION OF PARALLEL PLATE GEOMETRY TO THE REFLECTION OF GUIDED WAVES FROM A MAGNETIZED PLASMA

Experimental studies of the reflection of guided waves from a longitudinally magnetized plasma column were presented in Quarterly Progress Report No. 76, pp. 81-86. The power reflected during the afterglow of a pulsed argon discharge tube inserted in a section of S-band waveguide was studied as a function of magnetic field, electron density, and incident frequency. In conformity with the theory of propagation of electromagnetic waves in cold plasma, the condition for a maximum or minimum in reflection amplitude depended only on the dimensionless parameters $\alpha^2 = \frac{\omega_p^2}{\omega^2}$ and $\beta^2 = \frac{\omega_c^2}{\omega^2}$. Furthermore, in the α^2, β^2-plane, the locus of a given maximum (or minimum) formed a fairly straight line starting at the point $\alpha^2 = 0$, $\beta^2 = 1$ and extending in some cases as far as $\alpha^2 = 1$.

It was suggested at the time that reflection maxima could arise from constructive interference of waves off the two faces of the plasma region so that the loci plotted in the α^2, β^2-plane would correspond to curves of $k_z(\alpha^2, \beta^2)$ = constant, where k_z is the

wave number along the waveguide. Further experimental studies have shown, however, that the reflection characteristics at low densities and magnetic fields are determined primarily by a cavity mode that exists in the empty waveguide. The cylindrical metal sleeves or "chokes" which surround the plasma column outside the guide and prevent radiation losses, provide a chamber wide enough to support a trapped standing wave. The electric field of this mode is perpendicular to that of the normal guided wave and so is cut off in the region beyond the chokes. Resonances of the empty "cavity" have been found at frequencies of 2534, 3067, and 3480 Mc. At other frequencies an incident propagating wave is undisturbed but, just on either side of resonance, the impedance mismatch is considerable. This explains the double peaks in reflection observed near these frequencies at low electron densities.

The problem of understanding the reflection characteristics at high densities and at magnetic fields close to cyclotron resonance still remains. In this region, the plasma column itself could have an appreeiable index of refraction and become the principal reflecting agent. Indeed, the observed effect is a series of equally spaced maxima and minima strongly suggestive of an interference pattern. Partial agreement may be obtained by simply using the relation $k_z(\alpha^2, \beta^2) = \text{constant}$, where $k_z^2 = k_r^2 = \frac{\omega^2}{c^2}\left[1 - \frac{\alpha^2}{1-\beta}\right]$; that is, by considering a right circularly polarized wave propagating along the magnetic field. Unfortunately, pure circular waves cannot exist in a waveguide with perfectly conducting walls and a less more realistic model is required. The simplest geometry that includes guide effects is that of two parallel conducting plates infinite in extent and uniformly filled with homogeneous plasma. Consider the applied magnetic field, B_o, to be in the z-direction, which is parallel to the plates. The field equations governing this case have been presented by A. Bers.[1] Briefly, assuming the longitudinal and time dependence of the fields to be $e^{i(\omega t - k_z z)}$, a fourth-order scalar wave equation involving only transverse coordinates is obtained for the z-component of either $\vec{E}$ or $\vec{H}$. The particular advantage of the parallel plate geometry is that the wave functions are merely sums of sines and cosines and one can turn his attention immediately to the dispersion relation.

The solutions split into two separate clasese, symmetric and antisymmetric with respect to a plane midway between the plates. For the symmetric case, application of the condition that the tangential component of $\vec{E}$ vanish at the walls yields the dispersion relation

$$f_1 p_2 \cos(p_1 d) \sin(p_2 d) - f_2 p_1 \cos(p_2 d) \sin(p_1 d) = 0 \qquad (1)$$

Here 2d is the plate separation, p_1 and p_2 are transverse wave numbers given by the two roots of

$$p^4 + \left[k_o^2 \left(K_{||} + \frac{K_r K_\ell}{K_\perp} \right) - k_z^2 \left(\frac{K_{||}}{K_\perp} + 1 \right) \right] p^2 + \frac{K_{||}}{K_\perp} \left(k_o^2 K_r - k_z^2 \right) \left(k_o^2 K_\ell - k_z^2 \right) = 0, \qquad (2)$$

and the f_i are defined by

$$f_i = \frac{K_\perp}{k_z K_\times} \left[\frac{\left(k_o^2 K_\perp - k_z^2 \right) p_i^2}{\left(k_o^2 K_r - k_z^2 \right) \left(k_o^2 K_\ell - k_z^2 \right)} - 1 \right].$$

In the above we have used $k_o^2 = \frac{\omega^2}{c^2}$ as the frequency variable. The capital K's are various dielectric coefficients related to a and β by

$$K_{\substack{r \\ \ell}} = 1 - \frac{a^2}{1 \mp \beta}, \quad K_\perp = 1 - \frac{a^2}{1 - \beta^2}, \quad K_{||} = 1 - a^2 \text{ and } K_\times = \frac{i a^2 \beta}{1 - \beta^2}.$$

The above equations present a rather involved relation between the four variables a, β, k_o, and k_z. In principle, numerical results can be obtained by fixing the values of three of these parameters and varying the fourth until Eq. 1 is satisfied. Usually an iterative scheme of successive approximations based on the slope of the function in question is employed, but for the method to be effective, a reasonable initial guess as to the approximate location of a desired root must be made. This is especially true in the present problem with its discrete spectrum of transverse eigenfunctions providing an infinitude of roots that must be distinguished. In order to simplify the dispersion relation further and understand the various types of propagating modes, it is convenient to consider the limiting case in which $a^2 \to 0$, $\beta^2 \to 1$ but the ratio $\frac{a^2}{\beta^2 - 1} = \eta$ is arbitrary. The use of this limit is prompted by the fact that the observed loci of reflection maxima correspond roughly to the condition η = constant. The dielectric coefficients then take on the limiting values

$$K_r = 1 + 2\eta, \quad K_\ell = K_{||} = 1, \quad K_\perp = 1 + \eta \text{ and } K_\times = -i\eta.$$

Equation (2) for the p_i becomes

$$p^4 - \left[k_o^2 \left(1 + \frac{1+2\eta}{1+\eta} \right) - k_z^2 \left(\frac{1}{1+\eta} + 1 \right) \right] p^2 + \frac{1}{1+\eta} \left[k_o^2 (1+\eta) - k_z^2 \right] \left[k_o^2 - k_z^2 \right] = 0,$$

which factors directly giving

$$p_1^2 = k_o^2 - k_z^2 \quad \text{and} \quad p_z^2 = \frac{(1+2\eta) k_o^2 - k_z^2}{1 + \eta}. \qquad (3)$$

Finally, it turns out that

$$f_1 p_z = \frac{-k_o^2}{k_z l_z} \quad \text{and} \quad f_2 p_1 = \frac{-k_z}{p_1}$$

so that Eq. (1) simplifies to

$$p_1 \cos(p_1 d) \sin(p_z d) + \frac{k_z^2}{k_o^2} p_z \cos(p_z d) \sin(p_1 d) = 0 \tag{4}$$

with p_1 and p_2 given in (3). A similar relation with the sines and cosines interchanged applies to the antisymmetric case. In the regions where either p_1^2 or p_2^2 is negative, hyperbolic trigonometric functions are used. However, if both p_1 and p_2 are pure imaginary, Eq. 4 becomes

$$|p_1| \cosh(|p_1| d) \sinh(|p_z| d) + \frac{k_z^2}{k_o^2} |p_2| \cosh(|p_2| d) \sinh(|p_1| d) = 0,$$

which has no solution for real k_o and k_z.

Figure X-19 shows a diagram of the $\eta, \left(\frac{k_z}{k_o}\right)^2$-plane indicating the areas where propagation is possible. The line $\eta = 0$ corresponds to the empty waveguide and the line $\eta = -1$ to the plasma resonance condition $\frac{K_r K_\ell}{K_\perp} = \frac{1 + 2\eta}{1 + \eta} = \infty$. The left boundary provides the cutoff limit $k_z = 0$, and the line $\left(\frac{k_z}{k_o}\right)^2 = 1$ represents waves traveling with a phase velocity in the z-direction equal to the speed of light. All modes for $-1 < \eta < 0$ approach this limit as $k_o \to \infty$. Modes for $\eta > 0$ are seen to approach the limit $k_z^2 \to (1+2\eta)k_o^2$ but for $\eta < -1$, the ratio k_z/k_o can become arbitrarily large.

The cutoff limit $k_z/k_o \to 0$ is easily taken. For symmetric modes Eq. 4 becomes $p_1 \cos(p_1 d) \sin(p_2 d) = 0$ and yields two solutions

$$\cos(p_1 d) = 0, \quad \text{or} \quad k_o d = (2n-1)\frac{\pi}{z}$$

and $n = 1, 2, 3, \ldots$

$$\sin(p_2 d) = 0 \quad \text{or} \quad k_o d = \sqrt{\frac{1+\eta}{1+2\eta}}\, n\pi$$

The first solution corresponds to the TM or "ordinary" cutoff whereas the second gives the TE or "extraordinary" cutoff condition.

With the aid of a digital computer one can now proceed as follows: For a given value of η (starting at $k_z = 0$ and k_o = cutoff limit of desired mode) k_z can be increased by

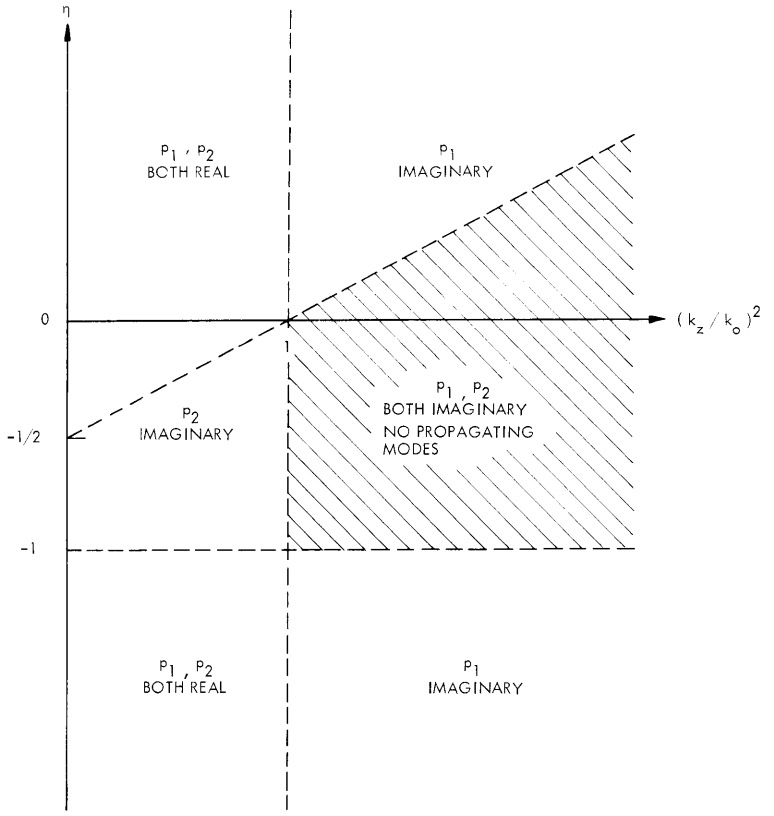

Fig. X-19. Properties of p_1 and p_2 in the η, $(k_z/k_d)^2$-plane.

increments and the iterative process employed to trace an entire curve relating k_o to k_z. Such a curve is not a proper dispersion relation because α and β are not varied along with k_o, but a collection of such curves provides the necessary starting values for proceeding away from the limit $\alpha^2 = 0$, $\beta^2 = 1$ out into the rest of the α^2, β^2-plane.

Typical results of this method are shown in Figs. X-20 and X-21 where curves corresponding to various values of k_z are presented for a fixed value of k_o. These should be compared with the experimentally observed loci of reflection maxima given in the previous report.[2] Figure X-20 is based on the lowest antisymmetric mode, which has the cutoff properties of a TE wave. No relation between the traces in Fig. X-20 and the experimental ones is evident. Figure X-21, which illustrates the lowest symmetric mode, is far more encouraging. At small values of α^2, these curves exhibit all the properties of the observed loci including the very crucial one that no curves lie in the

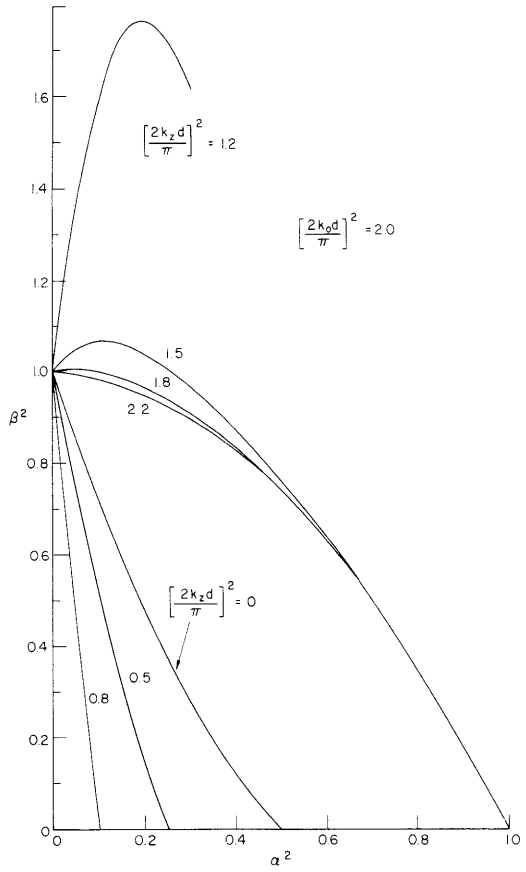

Fig. X-20. Lines of constant k_o and k_z for the antisymmetric mode.

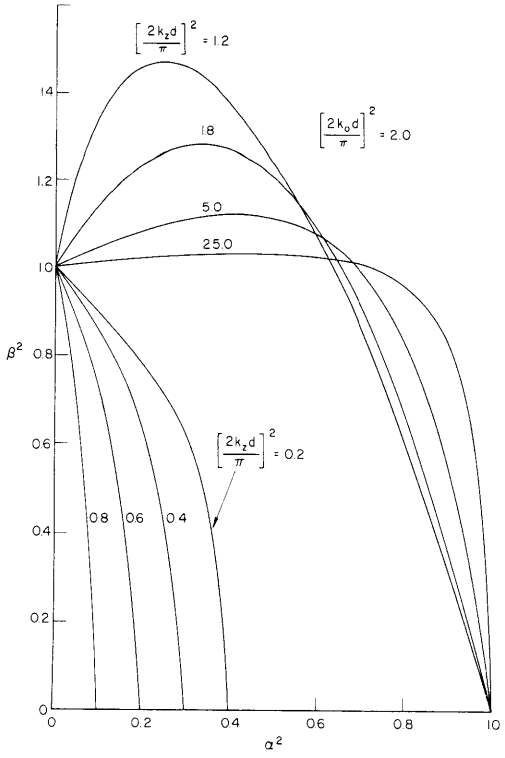

Fig. X-21. Lines of constant k_o and k_z for the symmetric mode.

region bounded by $\alpha^2+\beta^2 = 1$ and $\beta^2 = 1$. The only shortcoming is the bending of the curves as α^2 becomes significant; no such curvature was found in the experiment. In this connection it should be pointed out that the reported electron density was that of the plasma column itself and hence was greater than an average taken over the waveguide cross section. Furthermore, plots similar to those shown in Fig. X-20, taken at various values of k_o, show that as k_o increases the curves are straight over a larger range of α^2 before bending.

B. L. Wright

References

1. A. Bers in W. P. Allis, S. J. Buchsbaum and A. Bers, Waves in Anisotropic Plasmas (The M. I. T. Press, Cambridge, Mass., 1963), Section 10.3.1.

2. B. L. Wright, Quarterly Progress Report No. 76, Research Laboratory of Electronics, M. I. T., January 15, 1965, Fig. XIV-3, p. 83.